A codimension-two bifurcation organises the dynamics of the transition between multipotent and fate-specified cell states

Nathan Schofield[1], Saeed Farjami[2], Andrea Rocco[3,4],
Robert N. Kelsh[5], Jonathan H.P. Dawes[6*]

[1]*Mathematical Institute, University of Oxford, Oxford OX2 6GG*
[2]*Pirbright Institute, Ash Road, Pirbright, Woking, Surrey GU24 0NF*
[3]*School of Mathematics and Physics, University of Surrey, Guildford GU2 7XH*
[4]*School of Biosciences, University of Surrey, Guildford GU2 7XH*
[5]*Department of Life Sciences, University of Bath, Bath BA2 7AY*
[6]*Department of Mathematical Sciences, University of Bath, Bath BA2 7AY*

Keywords: bifurcation, gene expression, gene regulatory network, mathematical model, multipotency, oscillation, stem cell, symmetric bifurcation theory

Abstract

Understanding the process of fate specification, i.e. how multipotent stem cells are able to transition into one of several different cell types, is a central question in developmental biology.

In our previous work we proposed a mathematical model for this transition which, perhaps surprisingly, appeared generically to include an oscillatory regime in the path from multipotent cells to fate-specified states.

Here we carry out a detailed mathematical analysis of two variants of a generic gene regulatory network. We show how symmetry organises many aspects of the model behaviour and reveal the role of a specific codimension-two bifurcation point as an organising centre. The central role of symmetry implies that qualitatively equivalent results would be obtained regardless of the modelling details. The model-independent nature of our results makes them of substantial wider interest and is supported by numerical work. We conclude that the overall sequence of bifurcations that create and destroy the oscillations is generically and robustly organised by this codimension-two point.

In the stem cell context the persistence of the oscillatory regime augments the perspective suggested by Waddington's epigenetic landscape by highlighting the potentially dynamic nature of cell fate transitions.

1 Introduction

Understanding the mechanism by which multipotent cells select a single cell fate remains a central challenge in developmental biology. Although the biological details of how different fates are activated are likely to differ substantially between different populations of stem cells, let alone between different organisms, our understanding of development continues to rest on a relatively small number of animal models in which detailed genetic experimentation is possible. There is a very substantial literature on cell fate specification, stretching back over eighty years [33]. Waddington's early contributions remain relevant in the sense that they established a mental picture of the process of cell fate specification as being metaphorically similar to a ball rolling down an evolving landscape within which an increasing number of valleys, or channels are being formed, corresponding to different eventual final cell types. This paradigm remains central to the conceptual understanding of the field and the analysis of mathematical models for gene interaction [21, 34, 15, 22, 11].

One long-standing biological model system, which provided motivation for the mathematical models considered here, is the case of neural crest stem cells (NCSCs) in zebrafish. NCSCs are responsible for the formation in the embryo, among other alternatives, of the cells that result in black, blue and yellow-coloured pigment cells in the fish: these correspond to cell types referred to as melanophores, iridophores and xanthophores, respectively [4]. For this particular class of NCSCs

*Corresponding author: J.H.P.Dawes@bath.ac.uk

there is a long-running debate in the literature over two possible developmental mechanisms for cell fate specification, known as direct fate restriction (DFR) and progressive fate restriction (PFR), see [23, 14] and references therein. The difference between these two mechanisms is whether (the PFR case), or not (the DFR case), there exist partially fate-restricted intermediary cell states.

However, data on gene expression levels during development can usually only be obtained (for example by single-cell RNA sequencing) as a snapshot, by pausing development in the embryo at one specific point in time, destroying the embryo by separating cells and then attempting to reconstruct developmental trajectories through the analysis of the characteristics of the resulting overall population of stem cells [24]. The variation in this cell population arises through a range of stochastic environmental and other influences, resulting in some cells being further along the developmental journey than others at this single point in real time, while others lag behind. From the variations within this cell population, and a number of underlying assumptions, one can reconstruct the likely developmental histories of cells through estimation of a 'pseudotime' axis, followed by clustering that identifies distinct patterns of gene expression that correspond to the choices of different cell fates.

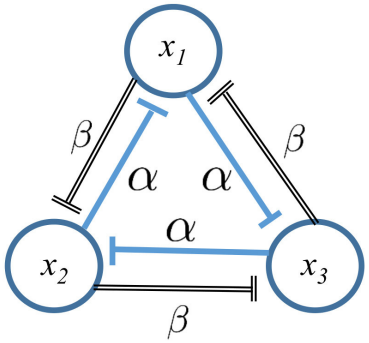

Figure 1: Schematic illustration of the GRN that forms the basis for our conceptual model for Cyclical Fate Restriction (CFR), comprising three TFs that mutually inhibit each other. The parameters α (blue inhibitory arrows) and β (black inhibitory arrows) describe the intensity of the cross-repressive inhibitory influences in the two directed rings of inhibitory couplings.

Temporal fluctuations in gene expression levels hugely complicate the pseudotime reconstruction process. Indeed, if such temporal fluctuations are deterministic and inherent, rather than driven purely by stochastic factors, then this may place fundamental limits on the resolution of pseudotime reconstruction techniques [32]. But the challenge of reconciling the PFR and DFR hypotheses motivated us in previous work [23, 31] to propose a new hypothesis of a cyclical fate restriction (CFR) process that provides an alternative to both PFR and DFR and might help in resolving the discrepancies between different sets of experimental results. Specifically, if expression levels were oscillating in time, some of the instantaneous measurements recorded via single-cell RNA sequencing might capture cells at snapshots in which two or more TFs are instantaneously being expressed at significant levels; this could potentially then be interpreted as a more stable partially-fate-restricted cell state than actually is the case. Hence it is essential to understand the ability (or not) of a GRN to generate oscillatory signals in order to explore the set of likely measured gene expression outcomes generated by a particular underlying GRN behaviour. In this way, the presence of oscillations could reconcile the PFR and DFR paradigms. We discuss this issue at greater length elsewhere, in particular in [23, 31].

In our previous mathematical modelling work [16] which sought to provide a conceptual model to support the CFR hypothesis, we proposed a specific model for the interaction of three TFs, through mutual inhibition, to explore how mutual inhibition and competition between TFs might generate a sequence of transitions that captured the process of developmental specification of a single cell fate from an initially multipotent stem cell. In this paper we present a comprehensive analysis of the central model proposed there: we confirm mathematically results that were previously obtained only numerically, and we provide a wealth of detail on the bifurcation structure, dynamics, and

genericity of the model behaviour.

The GRN proposed in [16] takes the form shown in figure 1 where each TF inhibits the production of the other two, but at potentially different rates, denoted by the parameters α and β. For simplicity, we take the interactions to be symmetric in the sense that the three inhibitory interactions that form a 'clockwise' loop have the same interaction rates, denoted by α, and those that form the 'anticlockwise' loop do likewise, with a rate denoted by β. We therefore refer to this configuration as the 'cross-repressilator' or double repressilator, to contrast it with the single repressilator investigated by [13] that corresponds to the case where either α or β is zero. This exact symmetry is of course a modelling assumption made for mathematical and computational convenience, but because it simplifies the analysis it allows us to make substantial analytical progress and identify mathematical features that will persist when the symmetry is broken. We note that in general the use of mutual inhibition to formulate conceptual models to understand development, for example spatial patterning enabled by morphogen gradients [7, 2], is well-established.

The schematic of figure 1 obscures an important modelling element, noted in [16], as to whether, for the double repressilator, the inhibitory mechanism relies on both the TFs acting together, or if each inhibitory interaction can operate separately. We refer to the cooperative version in which (say) high levels of both x_2 and x_3 are required to suppress x_1 as the 'AND gate', and the alternative, in which a high level of the expression of either x_2 or x_3 is sufficient to suppress the expression of x_1, as the 'OR gate' version. Details of the derivation of appropriate models for these two cases are contained in [16] and the supplementary material associated with that paper.

The conceptual model for the 'OR gate' scenario takes the form of three nonlinear ODEs for TF expression levels $x_1(t)$, $x_2(t)$, $x_3(t)$:

$$\frac{\mathrm{d}x_1}{\mathrm{d}t} = b + \frac{g}{(1+\alpha x_2^h)(1+\beta x_3^h)} - dx_1\,, \tag{1}$$

$$\frac{\mathrm{d}x_2}{\mathrm{d}t} = b + \frac{g}{(1+\alpha x_3^h)(1+\beta x_1^h)} - dx_2\,, \tag{2}$$

$$\frac{\mathrm{d}x_3}{\mathrm{d}t} = b + \frac{g}{(1+\alpha x_1^h)(1+\beta x_2^h)} - dx_3\,. \tag{3}$$

On the right-hand-side of each equation the first term b represents a constant (low, and indeed rather unimportant) level of production of the TF, the second term represents the inhibitory influences of the other two TFs, motivated by the usual Hill function form with exponent h, hence a 'cross-repressilator', and the final term $-dx_i$ describes the natural degradation, at a rate d, of the TF x_i. It is easy to see that the inhibitory term in the ODE for a given variable x_i is small whenever the level of either of the other TFs is large. In terms of the GRN shown in Figure 1 this corresponds to each inhibitory influence acting independently. All the parameters are taken to be positive, and for simplicity we enforce a cyclical symmetry which is clear in the form of (24) - (26). The parameter g models the overall strength of the interactions between TFs and is our principal bifurcation parameter. g also sets the maximum value (which is g/d) of the expression level for each x_i. For low values of g we expect all three TFs to be expressed since there is little interaction between them, decoupling the differential equations from each other and allowing each to equilibrate at $x_i = g/d$. Then as g increases the inhibitory interaction strength increases. Then the stronger inhibition causes one TF to 'win out' over the others and drive expression levels towards one of a number of distinct and new equilibria (that therefore describe different cell fates).

The existence and stability of equilibria for (1) - (3) turn out to be remarkably robust to the exact choice of parameter values. We now very briefly review the behaviour of (1) - (3) as explored in detail in our previous work [16] in order to set the scene for the much more detailed analysis which is the subject of this paper. Typical one-parameter bifurcation diagrams varying the parameter g are shown in figure 2 for two different values of α. In both cases there is unique equilibrium point at small values of g which is stable and fully-symmetric in the sense that all its coordinates are equal: $x_1 = x_2 = x_3$. Numerical investigations show that it loses stability in a supercritical Hopf bifurcation as g increases, creating a stable periodic orbit that is indicated in the figure by plotting the maximum and minimum values that $x_1(t)$ (and hence also $x_2(t)$ and $x_3(t)$ by symmetry) attains

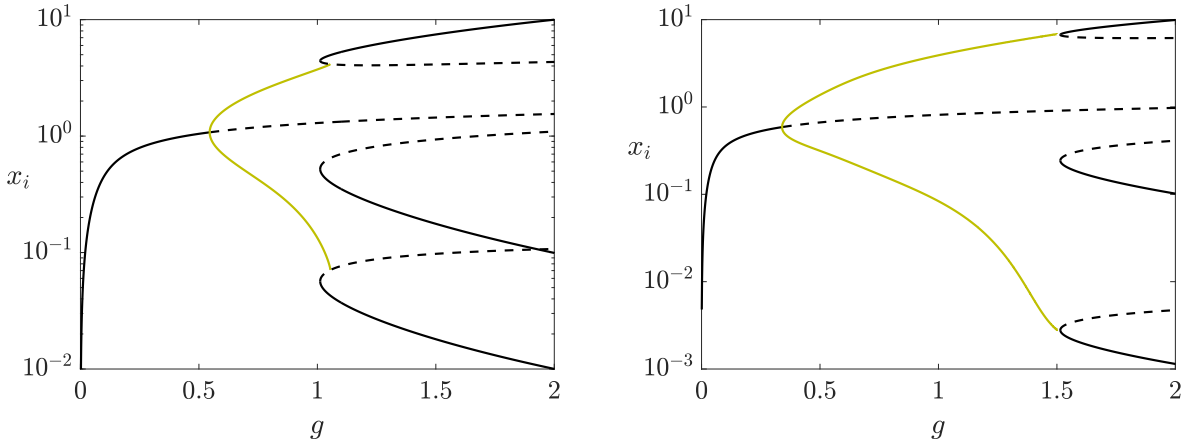

Figure 2: [From [16]] Numerically-computed one-parameter bifurcation diagrams for the system (1) - (3) varying the parameter g for two different fixed values of α. Stable and unstable equilibria are indicted by solid and dashed lines, respectively. The olive-coloured lines indicate the maximum and minimum values of x_i attained on the periodic orbit that is created in the Hopf bifurcation at $g \approx 0.5$. (a) $\alpha = 1.0$; (b) $\alpha = 9.0$. In both cases there are three saddle-node bifurcations at the same value of g due to symmetry. Other parameter values: $b = 0$, $\beta = 0.1$, $d = 0.2$, $h = 3$.

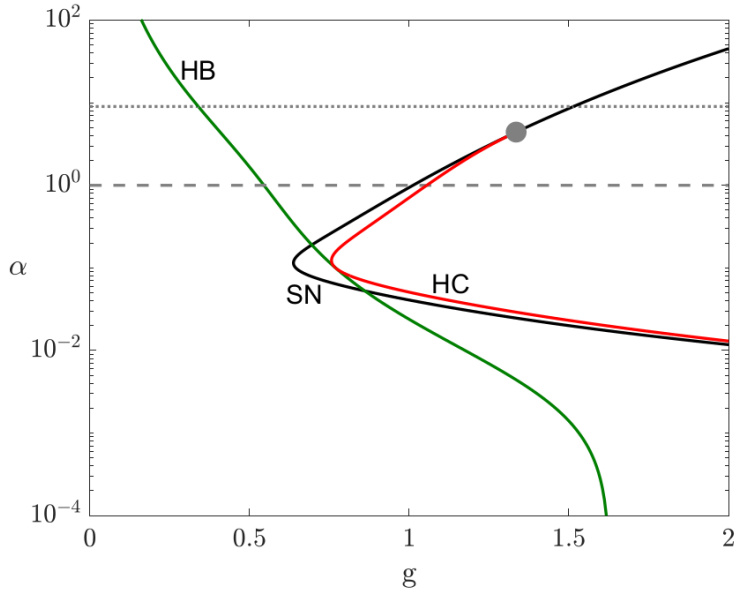

Figure 3: [From [16]] Numerically-computed two-parameter bifurcation diagram for (1) - (3) showing curves of codimension-one bifurcations in the (g, α) plane. The green curve labelled HB indicates a Hopf bifurcation from the symmetric equilibrium; the black curve labelled SN denotes a saddle-node bifurcation at which pairs of stable and saddle-type equilibria appear (3 pairs due to the symmetry); the red curve labelled HC indicates a heteroclinic bifurcation where the stable periodic orbit created to the right of the HB curve collides with saddle-type equilibria and disappears. The horizonal dashed and dotted lines correspond to the codimension-one bifurcation diagrams for the fixed values of $\alpha = 1.0$ and $\alpha = 9.0$ shown in figures 2(a) and 2(b), respectively. Other parameter values: $\beta = 0.1$, $b = 0$, $d = 0.2$, and $h = 3$.

on the orbit. For $\alpha = 1.0$ a set of three (symmetry-related) saddle-node bifurcations takes place at $g \approx 1$ and the periodic orbit then collides, in a standard global bifurcation, with the saddle-type equilibria that are created, leaving only the six new equilibria and the original fully-symmetric one at large g. For $\alpha = 9.0$ the bifurcation sequence is very similar except that the saddle-node bifurcations take place on the periodic orbit itself, i.e. a saddle-node on an invariant curve (SNIC) also known as a saddle-node on a periodic orbit (SNIPER) bifurcation, so that the new equilibria

appear precisely as the periodic orbit is destroyed.

The transition between these two bifurcation diagrams can be investigated numerically by computing a two-parameter bifurcation diagram in the (g, α) plane, for example as shown in figure 3. This reveals the existence of two codimension-two points. One of these, at which the transition between the global bifurcation and the SNIPER bifurcation, is indicated by the grey dot at approximately $(g, \alpha) \approx (1.4, 5.0)$ in figure 3 where the red and black curves meet. The second, and more important, codimension-two point appears to occur at precisely $\alpha = 0.1$ where the red and green curves meet and are tangent to each other, meaning that the periodic orbit would no longer exist in the corresponding one-parameter bifurcation diagram varying g at fixed $\alpha = \beta = 0.1$, since it is created in the Hopf bifurcation (green curve) and immediately disappears in the global bifurcation (red curve).

Analysis of the 'AND gate' model offers more possibilities since the model contains a larger number of parameters but the preliminary explorations presented in [16] showed that similar behaviour was possible, with the biologically interesting difference being that the oscillations in the intermediatary regime moved between states in which two of the three TFs were expressed (one at a high level and one at a medium level) rather than being purely dominated by a single TF. The resulting differentiated states at larger values of g also contained this mixture of two TFs rather than a single one dominating.

This paper is therefore concerned with understanding two issues: (i) the role of symmetry in organising the various features of the bifurcation diagrams 2 and 3 and (ii) the dependence of the details of the bifurcation structure on both values of the parameters b, d, h and β and on the function form of the nonlinear terms in (1) - (3). In section 2 we explore the role of symmetry for a large class of nonlinear ODEs that undergo a Hopf bifurcation with symmetry. In section 2.2 we deduce the normal form that governs the dynamics, and in section 2.3 we show that it describes exactly the bifurcations (Hopf, saddle-node, heteroclinic) that we observe in two-parameter bifurcation diagrams such as figure 3. Section 3 summarises the calculations that allow us to reduce the model ODEs to the normal form. The most algebraically intensive parts of these calculations are deferred to the Appendix, and the result is presented in section 3.1. This calculation then allows us, in sections 4 and 5, to explore two mathematical models in detail: the single-repressilator proposed by [13] and then the double-repressilator (1) - (3). In brief, we show that single-repressilator can only generate oscillations via a Hopf bifurcation, and these are then destroyed by a second Hopf bifurcation. Non-symmetric equilibria are not produced and so no sequence of events that would describe cell fate choice is available. In contrast, for the double-repressilator (section 5) we find that the Hopf bifurcation curve generically contains a codimension-two point at which the associated frequency passes through zero, and that this codimension-two point is an organising centre for the dynamics. The computation of the coefficients of the relevant normal form for (1) - (3) (i.e. the 'OR gate' configuration) reveals that the signs of the coefficients do not change over a wide range of relevant parameter values. This is discussed in section 5.1 and allows us to conclude that the bifurcation behaviour shown in figure 3 is entirely typical of the 'OR gate' version of the double-repressilator model. Section 5.2 presents analysis of the 'AND gate' version which shows similar kinds of behaviour but for which the mathematical analysis becomes more involved due to the additional model parameters and nonlinear terms. We conclude in section 6.

2 Dynamics with symmetry

In this section we summarise, briefly, well-known results for generic dynamics with symmetry that predict the structure of the normal form which we derive in the following subsections. The key aim of this section is to set out quite how much can be learned purely from symmetry and is therefore completely independent of the exact choice of the functional form of the terms in the differential equations such as (1) - (3). The presentation becomes a little intricate in places and is not required in order to appreciate the remainder of the paper, but we intend it to be sufficiently self-contained to be comprehensible. General references for bifurcation theory in the presence of symmetry include the textbooks [18], [20], and [6]. The classic reference for equivariant bifurcation theory remains

[19] which also presents detailed analysis relevant to the case at hand here (specifically, Chapter XIII Section 5 and Chapter XV Section 4) although these additional details are not required in order to understand our results.

2.1 $\mathbb{Z}_3$ and D_3 symmetry

A collection of first-order ODEs $\dot{\boldsymbol{x}} = \boldsymbol{g}(\boldsymbol{x}) \in \mathbb{R}^n$ is equivariant (symmetric) under the action of a group Γ if for all elements $\gamma \in \Gamma$, $\boldsymbol{g}(M_\gamma \boldsymbol{x}) = M_\gamma \boldsymbol{g}(\boldsymbol{x})$ where M_γ is a real $n \times n$ matrix that represents the element γ, i.e. the set of matrices $\{M_\gamma : \gamma \in \Gamma\} \subset GL(n, \mathbb{R})$ forms a (real) representation of the group Γ. Without loss of generality we can assume that the representation is a subgroup of $O(n)$ the group of orthogonal $n \times n$ matrices under matrix multiplication. The constraint of equivariance arises naturally if whenever $x(t)$ is a solution of the ODEs, $M_\gamma \boldsymbol{x}(t)$ is also a solution. That is, for any particular trajectory $\boldsymbol{x}(t)$, $M_\gamma \boldsymbol{x}(t)$ might be exactly the same trajectory, or it might be a different one - in which case this new solution is said to lie on the same group orbit as $\boldsymbol{x}(t)$.

We denote by $\mathbb{Z}_3$ the cyclic group with three elements, and by D_3 the symmetry group of an equilateral triangle, i.e. the group comprising its 3-fold rotation and reflections through lines joining midpoints of each side to the opposite corner. D_3 therefore has six elements. The cyclic group of order m and the symmetry group of a regular m-gon are similarly denoted $\mathbb{Z}_m$ and D_m. $\mathbb{Z}_m$ has m elements, and D_m has exactly $2m$ elements.

A representation of a group Γ is said to be *irreducible* if the $n \times n$ matrices M_γ do not leave a proper non-trivial subspace of $\mathbb{R}^n$ invariant (i.e. a subspace V which is neither just $\{0\}$ nor all of $\mathbb{R}^n$). If such a subspace V exists then the representation is reducible. Since we assume that $\{M_\gamma\} \subset O(n)$, if V is an invariant subspace then so is its complement $V^\perp$ and so the matrices M_γ are block-diagonal: one can analyse how they act separately on V and on $V^\perp$.

A representation of a group Γ is said to be *absolutely irreducible* if the only matrices that commute with all the matrices M_γ are real multiples of the identity matrix. It is well-known that the generic steady-state bifurcations from an equilibrium point at the origin, for a set of Γ-equivariant ODEs, correspond to the absolutely irreducible representations of Γ. The essence of the proof of that statement is to suppose the existence of a steady-state bifurcation in which the action of Γ on the eigenspace of the eigenvalue zero is not absolutely irreducible. Then it would be possible to perturb the bifurcation problem so that one of two things happened: either the dimension of the eigenspace for the eigenvalue zero was reduced, or the zero eigenvalues became purely imaginary eigenvalues, in complex conjugate pairs. In either case the fact that one could do this with an arbitrarily small perturbation to the bifurcation problem demonstrates that the original setting was not robust to small perturbations and therefore not generic. As a result in equivariant bifurcation theory we focus attention, for steady-state bifurcations, on the cases that arise when the symmetry group acts via an absolutely irreducible representation.

To make the rather abstract discussion of the previous paragraphs more digestible to readers unfamiliar with the language, we now work through how this applies to the representations of the groups $\mathbb{Z}_3$ and D_3 that arise for our setting, in detail.

The cyclic symmetry present in (1) - (3) can be expressed formally as equivariance with respect to the permutation representation (also known as the 'regular representation') of the group $\mathbb{Z}_3$. Denoting the abstract group elements of $\mathbb{Z}_3$ by $\{I, \rho, \rho^2\}$ we introduce the matrices

$$M_I = \begin{pmatrix} 1 & 0 & 0 \\ 0 & 1 & 0 \\ 0 & 0 & 1 \end{pmatrix}, \quad M_\rho = \begin{pmatrix} 0 & 0 & 1 \\ 1 & 0 & 0 \\ 0 & 1 & 0 \end{pmatrix}, \quad M_{\rho^2} = \begin{pmatrix} 0 & 1 & 0 \\ 0 & 0 & 1 \\ 1 & 0 & 0 \end{pmatrix}, \tag{4}$$

This representation of $\mathbb{Z}_3$ is reducible: the matrices all leave points in the 1D subspace $V_1 := \mathrm{span}\langle(1,1,1)^\perp\rangle$ invariant, and so V_1 and its 2D complement $V_2 \equiv V_1^\perp = \mathrm{span}\langle(2,-1,-1)^\perp, (0,-1,1)^\perp\rangle$, are proper non-trivial invariant subspaces. This action of $\mathbb{Z}_3$ on each of V_1 and $V_1^\perp$ is irreducible, though, so we expect bifurcations to be associated with each of V_1 and V_2, as we now show.

The constraint that the ODEs $\dot{\boldsymbol{x}} = \boldsymbol{g}(\boldsymbol{x})$ in $\mathbb{R}^3$ are $\mathbb{Z}_3$-equivariant under this representation of $\mathbb{Z}_3$ implies that we require

$$M_\gamma \boldsymbol{g}(\boldsymbol{x}) = \boldsymbol{g}\left(M_\gamma \boldsymbol{x}\right), \quad \forall\, \gamma \in \mathbb{Z}_3 \tag{5}$$

i.e. in terms of the individual coordinates $\boldsymbol{x} = (x_1, x_2, x_3)$ and components of the vector field $\boldsymbol{g} = (g_1, g_2, g_3)$, the constraints (5) imply that if $\dot{x}_1 = g_1(x_1, x_2, x_3)$ then the other two components of the vector field are related to g_1 by

$$\begin{aligned} \dot{x}_2 &= g_2(x_1, x_2, x_3) = g_1(x_2, x_3, x_1), \\ \dot{x}_3 &= g_3(x_1, x_2, x_3) = g_1(x_3, x_1, x_2). \end{aligned}$$

Differentiating (5) with respect to $\boldsymbol{x}$ we obtain

$$M_\gamma \, \mathbf{D}\boldsymbol{g} \,|_{\boldsymbol{x}} = \mathbf{D}\boldsymbol{g} \,|_{M_\gamma \boldsymbol{x}} \, M_\gamma \ , \quad \forall \, \gamma \in \mathbb{Z}_3 \tag{6}$$

which in general relates the Jacobian matrix $\mathbf{D}\boldsymbol{g}$ evaluated at the point $\boldsymbol{x}$ to the Jacobian matrix $\mathbf{D}\boldsymbol{g}$ evaluated at the point $M_\gamma \boldsymbol{x}$. In the case that $\boldsymbol{x}$ is fixed under all the matrices M_γ, i.e. $\boldsymbol{x} = M_\gamma \boldsymbol{x} = (x_0, x_0, x_0)$ for some value of x_0, i.e. points that lie along the subspace in which all three coordinates are equal, it provides a constraint on the form of the Jacobian evaluated at $\boldsymbol{x}$:

$$M_\gamma \mathbf{D}\boldsymbol{g} \,|_{\boldsymbol{x}} = \mathbf{D}\boldsymbol{g} \,|_{\boldsymbol{x}} M_\gamma \ , \quad \forall \, \gamma \in \mathbb{Z}_3 \tag{7}$$

and so $\mathbf{D}\boldsymbol{g}$ commutes with all the matrices M_γ. It is easy to see (by direct computation, or from the properties of circulant matrices) that the most general form of $\mathbf{D}\boldsymbol{g}$ that commutes with all the matrices in (4) is

$$\mathbf{D}\boldsymbol{g}|_{(x_0,x_0,x_0)} = \begin{pmatrix} a & b & c \\ c & a & b \\ b & c & a \end{pmatrix} \tag{8}$$

where the coefficients are partial derivatives, i.e. $a := \partial g_1/\partial x_1$, $b := \partial g_1/\partial x_2$, and $c := \partial g_1/\partial x_3$, all evaluated at the equilibrium point. As in the Appendix to Farjami et al [16], this implies that the eigenvalues $\lambda_1, \lambda_2, \lambda_3$ of the linearisation $\mathbf{D}\boldsymbol{g}$ in (8) are

$$\begin{aligned} \lambda_1 &= a + b + c \\ \lambda_{2,3} &= a - \frac{1}{2}(b + c) \pm \mathrm{i}\frac{\sqrt{3}}{2}(b - c) \, . \end{aligned} \tag{9}$$

There are therefore, generically, two distinct local bifurcation possibilities: when either $\lambda_1 = 0$ or when $\mathrm{Re}(\lambda_{2,3}) = 0$. For the first of these (associated to V_1), we would expect generically this steady-state instability to be a saddle-node bifurcation, although features of a particular set of ODEs might dictate that this was instead either a transcritical or a pitchfork bifurcation. For the second case (associated to V_2) we would generically expect a Hopf bifurcation to occur, as long as $\mathrm{Im}(\lambda_{2,3}) \neq 0$ at the bifurcation point.

2.1.1 Additional D_3 symmetry

In the case in which there is an additional symmetry operation that makes the full symmetry group the dihedral group D_3 rather than $\mathbb{Z}_3$, the regular representation of $D_3 = \{I, \rho, \rho^2, m, mp, m\rho^2\}$ on $\mathbb{R}^3$ is generated by the pair of matrices M_ρ and M_m:

$$M_I = \begin{pmatrix} 1 & 0 & 0 \\ 0 & 1 & 0 \\ 0 & 0 & 1 \end{pmatrix} , \quad M_\rho = \begin{pmatrix} 0 & 0 & 1 \\ 1 & 0 & 0 \\ 0 & 1 & 0 \end{pmatrix} , \quad M_m = \begin{pmatrix} 0 & 1 & 0 \\ 1 & 0 & 0 \\ 0 & 0 & 1 \end{pmatrix} , \tag{10}$$

As previously, D_3 acts reducibly on $\mathbb{R}^3$ and it acts irreducibly on each of the subspaces V_1 and V_2. The technical diffence from the $\mathbb{Z}_3$ case is that the action on V_2 is in addition now absolutely irreducible, not just irreducible. In the D_3-symmetric case, the most general form of $\mathbf{D}\boldsymbol{g}$ that commutes with all the matrices in (10) is

$$\mathbf{D}\boldsymbol{g}|_{(x_0,x_0,x_0)} = \begin{pmatrix} a & b & b \\ b & a & b \\ b & b & a \end{pmatrix} \tag{11}$$

where the coefficients are $a := \partial g_1/\partial x_1$, $b := \partial g_1/\partial x_2 = \partial g_1/\partial x_3$, all evaluated at the equilibrium point. The eigenvalues $\lambda_1, \lambda_2, \lambda_3$ of the linearisation $\mathbf{D}\boldsymbol{g}$ in (11) are therefore

$$\begin{aligned} \lambda_1 &= a + 2b \\ \lambda_2 = \lambda_3 &= a - b\,. \end{aligned}$$

In these cases both of the generic bifurcations are then steady-state in nature: one when $\lambda_1 = 0$ and another when $\lambda_2 = \lambda_3 = 0$. The second possibility is a double-zero bifurcation but it has codimension-one due to the D_3 symmetry. It is also apparent that this second D_3-symmetric case relates to the second $\mathbb{Z}_3$-symmetric case, since the imaginary parts of (9) vanish when $b = c$, so that the bifurcation conditions are identical.

2.2 Normal form for $\mathbb{Z}_3$-equivariant bifurcation

In the previous sections we discussed explicitly the permutation representation ('regular representation') of $\mathbb{Z}_3$ and D_3 and noted that it is reducible (i.e. not irreducible). Since generic bifurcations with symmetry are governed by irreducible representations, it is worth exploring the normal form for bifurcations associated with the 2D irreducible representation V_2. The most elegant way to do this is to use a set of orthogonal 2×2 rotation matrices, and there is a natural choice for these, most easily written in terms of the single complex coordinate $z = x + \mathrm{i}y \in \mathbb{C} \cong \mathbb{R}^2$. The element ρ is then represented by the complex rotation $\mathrm{e}^{2\pi\mathrm{i}/3}$, and hence the other non-identity element ρ^2 must be represented by $\mathrm{e}^{4\pi\mathrm{i}/3}$. The normal form $\dot{z} = F(z, \bar{z})$ for the bifurcation is constrained by equivariance:

$$\mathrm{e}^{2\pi\mathrm{i}/3} F(z, \bar{z}) = F(\mathrm{e}^{2\pi\mathrm{i}/3} z, \overline{\mathrm{e}^{2\pi\mathrm{i}/3} z}),$$

from which we can see that a term of the form $Az^r\bar{z}^s$ in $F(z, \bar{z})$, where r and s are non-negative integers, and A is a complex coefficient, will be equivariant only if

$$\mathrm{e}^{2\pi\mathrm{i}/3} A z^r \bar{z}^s = A \mathrm{e}^{2\pi(r-s)\mathrm{i}/3} z^r \bar{z}^s,$$

which holds only if

$$1 \equiv r - s \mod 3\,.$$

Hence the lowest-order terms correspond to the choices $(r, s) = (1, 0)$, $(0, 2)$, $(2, 1)$, for $1 \leq r+s \leq 3$, with no restriction on the form of the coefficient $A \in \mathbb{C}$ for each term. We conclude that the generic normal form for this bifurcation takes the form

$$\dot{z} = (p_1 + \mathrm{i}q_1)z + (p_2 + \mathrm{i}q_2)\bar{z}^2 + (p_3 + \mathrm{i}q_3)z|z|^2 + O(|z|^4) \tag{12}$$

where the coefficients p_j, q_j are real, and are functions of the original problem parameters. In the subsequent subsections we compute these coefficients in terms of the partial derivatives of the first component f of the original vector field and show that these explicit calculations automatically produce ODEs for $y_2(t)$ and $y_3(t)$ that are in the required form.

To derive the 2D normal form for the case of D_3, we note that the additional constraint of equivariance with respect to a reflection symmetry since as $(x, y) \mapsto (x, -y)$ corresponds to equivariance under the operation $z \mapsto \bar{z}$. This implies the additional constraint $\overline{F(z, \bar{z})} = F(\bar{z}, z)$, i.e for a term $Az^r\bar{z}^s$ we have that $\bar{A}\bar{z}^r z^s = A\bar{z}^r z^s$ and hence the additional constraint is that the coefficient A must be real. Therefore for a generic D_3-symmetric bifurcation corresponding to the 2D irreducible representation, the normal form is given by (12) but with all the coefficients $q_j = 0$. This turns out to be the case that applies here.

2.3 Dynamics of the normal form

We now analyse the dynamics of (12) and show that in addition to the Hopf bifurcation that occurs when $p_1 = 0$ and $q_1 \neq 0$ there are the saddle-node bifurcations of equilibria away from $z = 0$ and the global bifurcation, both qualitatively arranged as indicated in figure 3.

The calculations for these additional bifurcations are algebraically easiest to perform for a version of the normal form that has had further rescaling applied to it. This also enables us to check our results against previous work by [3], [17] and references therein, including [1] and [12]. We summarise these results in a reasonable level of detail in order to present a self-contained account here.

2.3.1 A note on the Hopf bifurcation

The normal form (12) applies at the bifurcation point where $p_1 = 0$. So far, we have been careful not to describe this as a Hopf bifurcation, although there is clearly a complex conjugate pair of eigenvalues crossing the imaginary axis. The issue is that the normal form for a Hopf bifurcation does not contain the $(p_2 + \mathrm{i}q_2)\bar{z}^2$ term; if it is a Hopf bifurcation that occurs at $p_1 = 0$ then we should be able to remove this quadratic term through a near-identity (and hence invertible) coordinate transformation, turning (12) into exactly the usual Hopf bifurcation normal form. In this subsection we show that this transformation is indeed possible if and only if $q_1 \neq 0$. This can be seen explicitly by setting $p_1 = 0$, making the near-identity change of coordinates

$$w(t) = z + \tilde{\gamma}_0 \bar{z}^2 + \tilde{\gamma}_1 z\bar{z} + \tilde{\gamma}_2 z^2 \,, \tag{13}$$

and choosing appropriate values for the complex coefficients $\tilde{\gamma}_j$ in order to remove the quadratic term in (35) in the derivation of an ODE for w which has locally topologically equivalent dynamics.

After substituting (13) into (35) we find that we can set $\tilde{\gamma}_0 = (q_2 - \mathrm{i}p_2)/(3q_1)$ and $\tilde{\gamma}_1 = \tilde{\gamma}_2 = 0$ to obtain the equivalent but simpler ODE

$$\dot{w} \;=\; \mathrm{i}q_1 w + \left(p_3 + \mathrm{i}q_3 - \frac{10(p_2^2 + q_2^2)}{9q_1}\mathrm{i}\right) w|w|^2 + O(w^4) \,, \tag{14}$$

which is the Hopf normal form. Two notable features emerge: first, that the contribution to the coefficient of the cubic term in (14) is purely imaginary, i.e. it is a contribution to the frequency of the periodic orbit but not to its magnitude. Second, the coefficient depends on p_2 and q_2 through the single combination $p_2^2 + q_2^2$, i.e. the (squared) magnitude of the quadratic coefficient $p_2 + \mathrm{i}q_2$, but does not depend on its phase. We can conclude also that the Hopf bifurcation is supercritical when $p_3 < 0$ and subcritical when $p_3 > 0$.

2.3.2 Rescaling

In order to investigate in detail the saddle-node and global bifurcations we first perform a rescaling. Starting from (12) we write

$$\hat{z} = \left(\frac{p_3^2 + q_3^2}{p_2^2 + q_2^2}\right)^{1/2} \mathrm{e}^{\mathrm{i}\psi} z, \qquad \text{and} \qquad \hat{t} = \frac{p_2^2 + q_2^2}{(p_3^2 + q_3^2)^{1/2}} t \,,$$

where $\psi = \frac{1}{3}\tan^{-1}(-q_2/p_2)$. Dropping the $\hat{}$s on z and t, this change of variables transforms (12) into the rescaled version [3]:

$$\dot{z} \;=\; \lambda z + \bar{z}^2 + \mathrm{e}^{\mathrm{i}\theta_0} z|z|^2 \,, \tag{15}$$

where the coefficient of the quadratic term is now unity, the coefficient of the cubic term has unit magnitude, and the new parameters λ and θ_0 are related to the original coefficients via

$$\lambda \equiv \mu + \mathrm{i}\omega = (p_1 + \mathrm{i}q_1)\frac{(p_3^2 + q_3^2)^{1/2}}{p_2^2 + q_2^2} \qquad \text{and} \qquad \theta_0 = \tan^{-1}(q_3/p_3) \,.$$

The normal form (15) captures three bifurcations of interest here: saddle-node bifurcations of equilibria away from the origin, a Hopf bifurcation from the equilbrium point at the origin, and a global bifurcation in which the periodic orbit collides with the saddle-type equilibria created in the saddle-node bifurcations. These correspond directly to the curves labelled SN, HB and HC in figure 3. The Hopf bifurcation is discussed in detail in section 2.3.1 above. We now present the details for the other two bifurcations, retaining the general form of (15) although our attention in what follows later will be on the case $q_j = 0$ for $j = 1, 2, 3$, i.e. $\theta_0 = 0$ or π.

2.3.3 Saddle-node bifurcation

Setting $\dot{z} = 0$ and multiplying (15) by $\bar{z}\mathrm{e}^{-\mathrm{i}\theta_0}$ we obtain

$$\rho z + z\zeta \;=\; -\mathrm{e}^{-\mathrm{i}\theta_0}\bar{z}^2\,, \tag{16}$$

where we define $\rho = \rho_1 + \mathrm{i}\rho_2 = \mathrm{e}^{-\mathrm{i}\theta_0}\lambda$ and $\zeta = |z|^2$. Multiplying this by its complex conjugate we obtain a real quadratic equation for ζ:

$$\zeta^2 + (\rho + \bar{\rho} - 1)\zeta + |\rho|^2 \;=\; 0\,,$$

which has solutions

$$\zeta \;=\; \frac{1}{2} - \rho_1 \pm \left(\frac{1}{4} - \rho_1 - \rho_2^2\right)^{1/2}\,, \tag{17}$$

and hence equilibria away from $\zeta = 0$ exist when $\rho_1 \le \frac{1}{4} - \rho_2^2$ and are created in a saddle-node bifurcation at $\rho_1 = \frac{1}{4} - \rho_2^2$ where ρ_1 and ρ_2 are the real and imaginary parts of ρ. Since $\lambda = \mathrm{e}^{\mathrm{i}\theta_0}\rho$ the shape of the curve in terms of $\lambda = \mu + \mathrm{i}\omega$ is a parabola rotated through an angle θ_0 about the origin. In terms of the real and imaginary parts of $\lambda = \mu + \mathrm{i}\omega$, solving the quadratic expression for μ explicitly we obtain

$$\mu \;=\; \frac{(2\omega\sin\theta_0 - 1)\cos\theta_0 \pm \sqrt{1 - 4\omega\sin\theta_0}}{2\sin^2\theta_0}\,,$$

which simplifies, taking appropriate choices of signs, to the following

$$\mu = \begin{cases} \frac{1}{4} - \omega^2 & \text{if } \theta_0 = 0 \\ \frac{1}{4}\left(1 + \tan^2\frac{\theta_0}{2}\right) - \omega\tan\frac{\theta_0}{2} - \omega^2 + O(\omega^3) & \text{if } -\pi/2 < \theta_0 < \pi/2 \\ -\frac{1}{4} + \omega^2 & \text{if } \theta_0 = \pi \\ -\frac{1}{4}\left(1 + \cot^2\frac{\theta_0}{2}\right) - \omega\cot\frac{\theta_0}{2} + \omega^2 + O(\omega^3) & \text{if } \pi/2 < \theta_0 < 3\pi/2 \end{cases} \tag{18}$$

showing that the SN curve is symmetric about $\omega = 0$ only when $\theta_0 = 0$ or π. The above discussion has considered only the modulus of z; we turn now to its argument. Since (16) implies also that

$$\bar{z}^3 \;=\; -\lambda\zeta - \mathrm{e}^{\mathrm{i}\theta_0}\zeta^2\,, \tag{19}$$

we see that generically there are three distinct values for the argument of z, for each of the choices of $\pm$ in (17), and hence three symmetrically-related saddle-node bifurcations occur on the line SN given by $\rho_1 = \frac{1}{4} - \rho_2^2$.

2.3.4 Global bifurcation

To locate the global bifurcation we observe that if we neglect the cubic term in (15) and set $\mu = 0$ the system is Hamiltonian, i.e. writing $z = u + \mathrm{i}v$ and

$$H_0(u, v) \;=\; -\frac{\omega}{2}(u^2 + v^2) + u^2 v - \frac{1}{3}v^3\,, \tag{20}$$

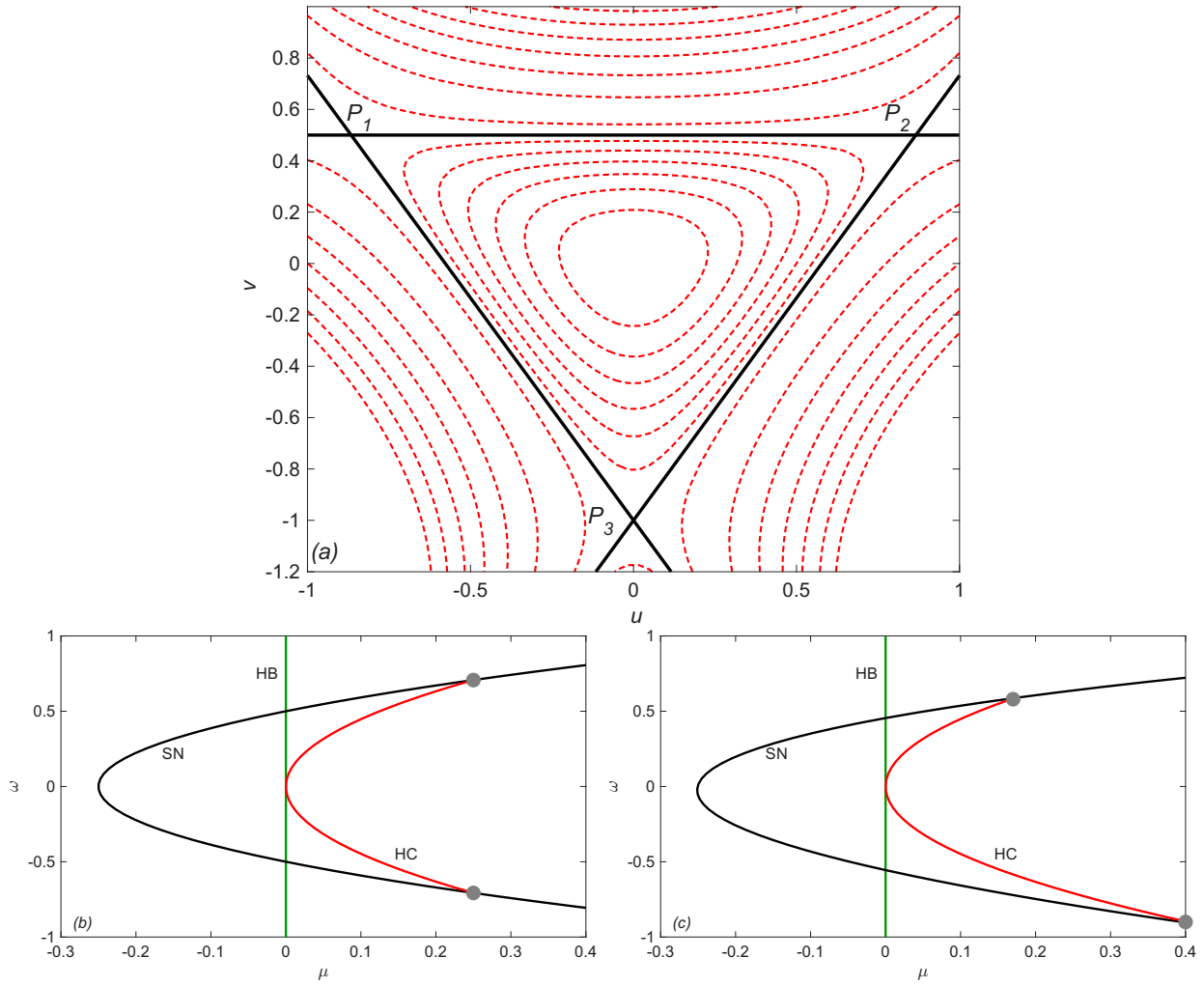

Figure 4: (a) Sketch of sets $H_0 = \text{const.}$ in the (u, v) plane for the case $\omega = 1$. Solid (black) lines denote the set $H = -1/6$ which contains the three saddle points at $(\pm\sqrt{3}/2, 1/2)$ and $(0, -1)$ and denoted P_1, P_2 and P_3 respectively. For $\omega > 0$ trajectories rotate anticlockwise around the origin. (b) Sketch of the curves along which Hopf ('HB', green), saddle-node ('SN', black) and global heteroclinic ('HC', red) bifurcations occur, near $(\mu, \omega) = (0, 0)$, in the case $\theta_0 = \pi$. Grey dots indicate codimension-two points where the heteroclinic and saddle-node bifurcation curves collide. (c) As for (b) but in the case $\theta_0 = \pi - 0.1$.

we have

$$\dot{u} = \partial H_0/\partial v\,, \qquad \dot{v} = -\partial H_0/\partial u\,,$$

and hence $\mathrm{d}H_0/\mathrm{d}t = 0$ along trajectories. This guarantees the existence of the saddle-saddle connecting orbits on which $H_0 = -\omega^2/6$ since the level sets of H_0 are as shown in figure 4(a).

A necessary condition for the preservation of these saddle-saddle orbits when $\mu \neq 0$ and the cubic terms are added back in is that the net change in H_0 along the orbit is zero, leading to the condition

$$\Delta H_0 \equiv \int_{(-\sqrt{3}\omega/2,\omega/2)}^{(\sqrt{3}\omega/2,\omega/2)} \mathrm{d}H_0 \;=\; 0\,, \tag{21}$$

where the integral is taken along the horizontal solid line between the saddle points at P_1 and P_2, i.e. $(\pm\sqrt{3}\omega/2, \omega/2)$. The constraint (21) can be approximated at leading order in μ and z by writing

$$\frac{\mathrm{d}H_0}{\mathrm{d}t} \;=\; \frac{\partial H_0}{\partial u}\dot{u} + \frac{\partial H_0}{\partial v}\dot{v}\,,$$

and using the full form of (15), taking the real and imaginary parts to deduce expressions for $\dot{u}$ and $\dot{v}$. We obtain

$$\begin{aligned}\Delta H_0 &\approx \frac{1}{2}\int_{-\sqrt{3}\omega/2}^{\sqrt{3}\omega/2}\left[\omega\mu + \left(u^2+\frac{\omega^2}{4}\right)(2u\sin\theta_0+\omega\cos\theta_0)\right]\,\mathrm{d}u\,,\\ &\approx \frac{\sqrt{3}}{4}\omega^2\left(2\mu+\omega^2\cos\theta_0\right)=0\,. \end{aligned} \tag{22}$$

Hence, for small μ and ω, the saddle-saddle connecting orbit persists (and hence the global heteroclinic bifurcation occurs) close to the curve $\mu = -\frac{1}{2}\omega^2\cos\theta_0$.

The overall arrangement of bifurcation curves for small (μ,ω) is therefore as shown in figure 4(b) and (c) for the cases $\theta_0=\pi$ and $\theta_0=\pi-0.1$, respectively, illustrating how the symmetry of the SN curve around the line $\omega=0$ is broken when $\theta_0\notin\{0,\pi\}$. This therefore qualitatively explains the bifurcation structure deduced numerically in earlier work and shown in figure 3, where the bifurcation parameter μ must decrease as g increases.

2.3.5 Secondary Hopf bifurcation

We note in passing that there is also the possibility of a secondary Hopf bifurcation from the equilibria (described by (17) and (19)) that appear away from the origin. The condition that the trace of the Jacobian matrix vanishes, necessary for Hopf bifurcation, implies

$$\mu + 2\zeta\cos\theta_0 \;=\; 0\,,$$

which simplifies to the condition

$$(2\omega\cos\theta_0-\mu\sin\theta_0)^2+(\mu\cos\theta_0+1)^2 \;=\; 1\,, \tag{23}$$

which describes an ellipse in the (μ,ω) plane that always passes through the origin and lies entirely in $\mu\le 0$ when $\theta_0=0$. The additional requirement, that the determinant of the Jacobian matrix is positive, leads to the inequality $\zeta+\rho_1>1/2$. Hence for small θ_0 there is no part of the ellipse (23) on which a Hopf bifurcation occurs. Further calculations show that the ellipse meets the saddle-node bifurcation curve SN at codimension-two Takens–Bogdanov points given by

$$\rho_2 \;=\; \frac{1}{2}\left(\tan\theta_0 \pm \sqrt{\tan^2\theta_0-3}\right)\,.$$

Hence no Takens–Bogdanov points exist, and there is no secondary Hopf bifurcation, when $\tan^2\theta_0<3$, i.e. for $-\pi/3<\theta_0<\pi/3$ and $2\pi/3<\theta_0<4\pi/3$.

3 Reduction from the ODEs in $\mathbb{R}^3$ to the 2D normal form

In the previous section we demonstrated that the restrictions imposed by symmetry imply that the normal form for the bifurcation is exactly (12). In this section we directly connect the ODEs $\dot{\boldsymbol{x}}=\boldsymbol{g}(\boldsymbol{x})$ in $\mathbb{R}^3$ and the normal form (12) at the bifurcation point where $Re(\lambda_{2,3})=0$ by carrying out the centre manifold reduction explicitly. This enables us to relate the coefficients (p_j,q_j) for $j=1,2,3$ in the normal form directly to the derivatives of $\boldsymbol{g}(\boldsymbol{x})$. This is a necessary intermediate step in our overall goal to relate the symmetric bifurcation theory from previous subsections to the ODEs for the model (1) - (3) and hence apply the above theory to the numerical results obtained in [16] (and, indeed, the results apply not just to the specific model chosen there). [16] start from a system of ODEs in $\mathbb{R}^3$ that is equivariant under the permutation action of the group $\mathbb{Z}_3$:

$$\dot{x}_1 \;=\; g_1(x_1,x_2,x_3), \tag{24}$$

$$\dot{x}_2 \;=\; g_2(x_1,x_2,x_3) \;=\; g_1(x_2,x_3,x_1), \tag{25}$$

$$\dot{x}_3 \;=\; g_3(x_1,x_2,x_3) \;=\; g_1(x_3,x_1,x_2). \tag{26}$$

Further, we assume the existence of a symmetrical equilibrium point (x_0, x_0, x_0) that undergoes a linear instability. As in the Appendix to [16], the eigenvalues $\lambda_1, \lambda_2, \lambda_3$ of the linearisation take the form

$$\begin{aligned} \lambda_1 &= a + b + c \\ \lambda_{2,3} &= a - \frac{1}{2}(b+c) \pm \mathrm{i}\frac{\sqrt{3}}{2}(b-c) \end{aligned}$$

where the coefficients are $a \equiv \partial g_1/\partial x_1$, $b \equiv \partial g_1/\partial x_2$, and $c \equiv \partial g_1/\partial x_3$, all evaluated at the equilibrium point. We assume in what follows that $\lambda_1 < 0$, but note that a Hopf bifurcation arises when $2a = b + c$, and, further, that $\lambda_2 = \lambda_3 = 0$ arises when $a = b = c$. These latter conditions therefore define a codimension-2 bifurcation point at which there are two zero eigenvalues of the Jacobian matrix evaluated at the equilibrium point. This can be interpreted, loosely speaking, as a codimension-two point in parameter space at which the frequency of the periodic orbits that are produced by the Hopf bifurcation becomes zero.

On symmetry grounds, or by computing directly from (24) - (26), the Jacobian matrix takes the form

$$Dg|_{(x_0,x_0,x_0)} = \begin{pmatrix} a & a & a \\ a & a & a \\ a & a & a \end{pmatrix},$$

which has eigenvalues and (un-normalised) eigenvectors given by

$$\lambda_1 = 3a, \quad \mathbf{v}_1 = \begin{pmatrix} 1 \\ 1 \\ 1 \end{pmatrix}; \qquad \lambda_2 = 0, \quad \mathbf{v}_2 = \begin{pmatrix} 2 \\ -1 \\ -1 \end{pmatrix}; \qquad \lambda_3 = 0, \quad \mathbf{v}_3 = \begin{pmatrix} 0 \\ -1 \\ 1 \end{pmatrix}.$$

These indicate that the equilibrium point has a one-dimensional stable subspace $\mathbb{E}^s$ spanned by $\mathbf{v}_1$ and a two-dimensional centre subspace $\mathbb{E}^c$ spanned by $\mathbf{v}_2$ and $\mathbf{v}_3$. We have not normalised the eigenvectors in order to avoid the need to carry around factors of $\sqrt{3}$, $\sqrt{6}$, and $\sqrt{2}$ in what follows; we will instead rescale appropriately at a later stage in the calculation.

To analyse the dynamics near the equilibrium point (x_0, x_0, x_0) we therefore introduce new variables $(y_1(t), y_2(t), y_3(t))$ that are assumed to remain small, allowing us to Taylor expand and consider just the first few polynomial terms in the $y_j(t)$ variables. Explicitly, we write

$$\begin{pmatrix} x_1(t) \\ x_2(t) \\ x_3(t) \end{pmatrix} = \begin{pmatrix} x_0 \\ x_0 \\ x_0 \end{pmatrix} + y_1(t)\mathbf{v}_1 + y_2(t)\mathbf{v}_2 + y_3(t)\mathbf{v}_3 = \begin{pmatrix} x_0 + y_1 + 2y_2 \\ x_0 + y_1 - y_2 - y_3 \\ x_0 + y_1 - y_2 + y_3 \end{pmatrix}. \tag{27}$$

Differentiating these expressions with respect to time and solving for $\dot{y}_1(t)$, $\dot{y}_2(t)$, and $\dot{y}_3(t)$ we obtain

$$\begin{aligned} \dot{y}_1 &= \frac{1}{3}\left(\dot{x}_1 + \dot{x}_2 + \dot{x}_3\right), \\ \dot{y}_2 &= \frac{1}{6}\left(2\dot{x}_1 - \dot{x}_2 - \dot{x}_3\right), \\ \dot{y}_3 &= \frac{1}{2}\left(\dot{x}_3 - \dot{x}_2\right), \end{aligned}$$

from which we can obtain ODEs for the y_j variables by substituting in the right-hand sides of the ODEs for $x_i(t)$ given by (24) - (26). Since by equivariance, explicitly the relations (25) - (26) which relate the forms of g_2 and g_3 directly to g_1, we change notation and define $f(x_1, x_2, x_3) := g_1(x_1, x_2, x_3)$. Hence

$$\dot{y}_1 = \frac{1}{3}\Big[f(x_1, x_2, x_3) + f(x_2, x_3, x_1) + f(x_3, x_1, x_2)\Big] \tag{28}$$

$$\dot{y}_2 = \frac{1}{6}\Big[2f(x_1, x_2, x_3) - f(x_2, x_3, x_1) - f(x_3, x_1, x_2)\Big] \tag{29}$$

$$\dot{y}_3 = \frac{1}{2}\Big[f(x_3, x_1, x_2) - f(x_2, x_3, x_1)\Big]. \tag{30}$$

Since we are working locally and (by assumption) f is real analytic in a neighbourhood of the bifurcation point, we continue by expanding f in Taylor series in the usual way. We introduce the notation $f_i := \partial f(x_1, x_2, x_3)/\partial x_i$, for $i = 1, \ldots, 3$, meaning that this is the partial derivative with respect to the i^{th} argument of the function. Similarly we define $f_{ij} := \partial^2 f/\partial x_i \partial x_j$ and $f_{ijk} := \partial^3 f/\partial x_i \partial x_j \partial x_k$ for $i, j, k \in \{1, 2, 3\}$. Indices may be different, or equal. We also denote by $\boldsymbol{\eta}$ the combination $\boldsymbol{\eta} := y_1\mathbf{v}_1 + y_2\mathbf{v}_2 + y_3\mathbf{v}_3$ so that the components of $\boldsymbol{\eta}$ are given by

$$\boldsymbol{\eta} \equiv (\eta_1, \eta_2, \eta_3) = (y_1 + 2y_2, y_1 - y_2 - y_3, y_1 - y_2 + y_3)\,. \tag{31}$$

Then the Taylor series of $f(x_1, x_2, x_3)$ at the equilibrium point (x_0, x_0, x_0) can be written as

$$f(x_1, x_2, x_3) \;=\; f(x_0, x_0, x_0) + \eta_1 f_1 + \eta_2 f_2 + \eta_3 f_3 + Q(\eta_1, \eta_2, \eta_3) + C(\eta_1, \eta_2, \eta_3), \tag{32}$$

where the terms that are quadratic in $\boldsymbol{\eta}$ are

$$Q(\eta_1, \eta_2, \eta_3) \;=\; \frac{1}{2}\eta_1^2 f_{11} + \frac{1}{2}\eta_2^2 f_{22} + \frac{1}{2}\eta_3^2 f_{33} + \eta_1\eta_2 f_{12} + \eta_2\eta_3 f_{23} + \eta_1\eta_3 f_{13}, \tag{33}$$

and the terms that are cubic in $\boldsymbol{\eta}$ are

$$\begin{aligned} C(\eta_1, \eta_2, \eta_3) \;=\; & \frac{\eta_1^3}{6} f_{111} + \frac{\eta_2^3}{6} f_{222} + \frac{\eta_3^3}{6} f_{333} + \frac{\eta_1\eta_2^2}{2} f_{122} + \frac{\eta_2\eta_3^2}{2} f_{233} + \frac{\eta_3\eta_1^2}{2} f_{311} \\ & + \frac{\eta_1\eta_3^2}{2} f_{133} + \frac{\eta_2\eta_1^2}{2} f_{112} + \frac{\eta_3\eta_2^2}{2} f_{233} + \eta_1\eta_2\eta_3 f_{123}\,. \end{aligned} \tag{34}$$

We now follow a standard approach consisting of the following steps:

- Substitute the Taylor series (32) into (28) - (30).
- Replace the η_j variables on the right-hand sides by the linear combinations of the y_j defined in (31).
- Observe that, since $Re(\lambda_1) < 0$ is bounded away from zero near the bifurcation point of interest, $\dot{y}_1$ can be assumed to be small, and hence the ODE for y_1 yields (implicitly) an expression $y_1 = F(y_2, y_3)$ that defines the centre manifold at the bifurcation point.
- Solve to obtain the leading order terms in $F(y_2, y_3)$ and substitute these for y_1 in the $\dot{y}_2$ and $\dot{y}_3$ equations.
- Simplify the resulting ODEs for y_2 and y_3 and rescale, introducing the variable $z \equiv u_2 + \mathrm{i}u_3 := y_2 + \mathrm{i}\sqrt{3}y_3$ in order to bring the normal form precisely into the form (12) as anticipated from the general discussion presented in section 2.2.

The details of these calculations are given in the Appendix (see supplementary material). Section A.1 treats the terms of linear and quadratic orders in $\boldsymbol{\eta}$, i.e. the linear terms in (32) and the terms in (33). This section also shows that the leading-order form of F is quadratic which indicates that the terms containing a factor of y_1 in (33) are in fact of cubic or higher order in (y_2, y_3). Section A.2 treats the cubic terms.

3.1 Normal form

Having followed the steps outlined above (and presented in detail in the Appendix), we obtain the normal form (12) as predicted on symmetry grounds, up to and including terms at cubic order in z:

$$\dot{z} \;=\; (p_1 + \mathrm{i}q_1)z + (p_2 + \mathrm{i}q_2)\bar{z}^2 + (p_3 + \mathrm{i}q_3)z|z|^2 \tag{35}$$

where now the coefficients are given explicitly, in terms of the derivatives of f, by the following expressions:

$$p_1 := \frac{1}{2}\left(2f_1 - f_2 - f_3\right), \tag{36}$$

$$q_1 := \frac{\sqrt{3}}{2}(f_2 - f_3), \tag{37}$$

$$p_2 := \frac{1}{4}\left(2f_{11} - 2f_{12} - 2f_{13} - f_{22} - f_{33} + 4f_{23}\right), \tag{38}$$

$$q_2 := \frac{\sqrt{3}}{4}(f_{22} - f_{33} - 2f_{12} + 2f_{13}), \tag{39}$$

$$p_3 := \frac{1}{4}\left[2f_{111} - 3f_{112} + 3f_{122} + 3f_{133} - f_{222} - 3f_{311} - f_{333} - \frac{(4f_{11} + 2f_{12} + 2f_{13} - 4f_{23} - 2f_{22} - 2f_{33})(f_{11} + f_{22} + f_{33} - f_{12} - f_{13} - f_{23})}{f_1 + f_2 + f_3}\right], \tag{40}$$

$$q_3 := \frac{\sqrt{3}}{4}\left[f_{112} + f_{133} - f_{122} + f_{222} - 2f_{223} + 2f_{233} - f_{311} - f_{333} + \frac{(2f_{33} - 2f_{22} + 2f_{13} - 2f_{12})(f_{11} + f_{22} + f_{33} - f_{12} - f_{13} - f_{23})}{f_1 + f_2 + f_3}\right], \tag{41}$$

While the linear and quadratic terms depend, respectively, on the first and second derivatives of the original nonlinearity $f(x_1, x_2, x_3)$, we note that the coefficients p_3 and q_3 depend on both the second and third derivatives of f.

Importantly, we remark that if we imposed the additional symmetry that exchanges x_2 and x_3 while leaving x_1 unchanged, thus changing the symmetry group from $\mathbb{Z}_3$ to D_3, then we would deduce that the derivatives for which all subscripts are either 2 or 3 would be equal, i.e. $f_2 = f_3$, $f_{22} = f_{33}$, $f_{222} = f_{333}$ and $f_{223} = f_{233}$. (But note that it is not the case in general that with this additional symmetry $f_{23} = f_{22}$). As a result, in the D_3 case the imaginary parts of the normal form coefficients will vanish, i.e. $q_1 = q_2 = q_3 = 0$ and so all the coefficients of terms in the normal form will be real. This agrees with the general theory set out above in section 2.1 and specifically also at the end of section 2.2 where we noted that indeed the D_3-symmetric case the normal form coefficients are all constrained to be real.

4 Single-repressilator dynamics

In this section we give the first explicit example, computing the normal form coefficients p_j, q_j for the repressilator proposed by [13]. We show three things: that a pair of Hopf bifurcations from the symmetric equilibrium appears if h is sufficiently large, that the frequencies associated with the Hopf bifurcations are always non-zero and so it is not possible to find codimension-two bifurcation points of the type associated to the normal form (12), and that both Hopf bifurcations are always supercritical. Taken together, these facts show that dynamics of the single-repressilator model is not capable of displaying the set of transitions that describe the CFR paradigm.

Motivated directly by [13] we consider the function $f(x_1, x_2, x_3)$, equivalently $g_1(x_1, x_2, x_3)$ in (24), given by

$$f(x_1, x_2, x_3) = b + \frac{g}{1 + \alpha x_2^h} - dx_1, \tag{42}$$

where α, b, d, and g are positive parameters, and $h > 1$. Since $dx_0 - b$ and $g/(1 + \alpha x_0^h)$ are strictly increasing and decreasing functions of x_0, respectively, it is clear graphically that for all combinations of (positive) parameter values there is a unique symmetric equilibrium point (x_0, x_0, x_0) for the single-repressilator system. We observe that the partial derivatives of f are

$$f_1 = -d, \qquad f_2 = \frac{-\alpha g h x_2^{h-1}}{(1 + \alpha x_2^h)^2}, \qquad f_3 = 0.$$

There is therefore no possibility of a steady-state bifurcation from the symmetric equilibrium point (x_0, x_0, x_0) since $f_1 + f_2 + f_3$ is always negative. Necessary conditions for the symmetric equilibrium point to undergo a Hopf bifurcation are

$$dx_0 = b + \frac{g}{1+\alpha x_0^h} \qquad \text{and} \qquad 2d = \frac{\alpha g h x_0^{h-1}}{(1+\alpha x_0^h)^2}\,. \tag{43}$$

Combining these, we deduce that a Hopf bifurcation occurs when

$$x_0 = x_{HB\pm} \;=\; \frac{b}{d} + \frac{g}{d}\left(\frac{1}{2} - \frac{1}{h}\right) \pm \frac{1}{d}\sqrt{g^2\left(\frac{1}{2}-\frac{1}{h}\right)^2 - \frac{2bg}{h}}\,, \tag{44}$$

and for this expression to be real we require

$$h > \left(\frac{1}{2} + \frac{b}{g} - \sqrt{\frac{b}{g}\left(1+\frac{b}{g}\right)}\right)^{-1}\,. \tag{45}$$

When, as we are assuming, $b > 0$ is small, the right hand side is slightly greater than 2, with (45) becoming the inequality $h > 2$ when $b = 0$. From the first part of (43) we see also that

$$\left.\frac{\mathrm{d}g}{\mathrm{d}x}\right|_{x_0} \;=\; d(1+\alpha x_0^h) + \frac{\alpha g h x^{h-1}}{1+\alpha x^h} > 0\,,$$

so $dx/dg|_{x_0}$ is also always positive, and hence $x_0(g)$ is a strictly increasing function. So $x_{HB-} < x_{HB+}$ implies that the corresponding values of g at which the Hopf bifurcation occur are also ordered so that $g_{HB-} < g_{HB+}$ always, and the equilibrium point (x_0, x_0, x_0) is unstable in the interval $g_{HB-} < g < g_{HB+}$.

When $b = 0$ the expressions (44) for the location of the Hopf bifurcations become

$$x_{HB\pm} \;=\; 0, \quad \frac{g}{d}\left(1 - \frac{2}{h}\right)\,,$$

which are valid only when $h > 2$ and show that we expect one Hopf bifurcation to occur close to $x_0 = g = 0$ when b is small, and that the location of the other does not depend, at leading order, on b when b is small.

Turning to the nonlinear development of the instability, from the results of section 3.1 we find that at the Hopf bifurcations at $g_{HB\pm}$ the normal form coefficients are

$$q_1 \;=\; -\frac{\sqrt{3}\alpha g h x_{HB\pm}^{h-1}}{2(1+\alpha x_{HB\pm}^h)^2} < 0\,,$$

which shows that this is always a standard Hopf bifurcation – the double-zero eigenvalue case in which q_1 vanishes cannot occur – and

$$p_3 \;=\; -\frac{1}{4}f_{222} + \frac{f_{22}^2}{3f_2} \tag{46}$$

since $2f_1 = f_2$. After some algebra we obtain

$$p_3 \;=\; -\frac{d^2}{3\alpha g h}\left[(h-1)(h+2)x_{HB\pm}^{-h-1} + 4\alpha(h^2-1)x_{HB\pm}^{-1} + \alpha^2(h+1)^2 x_{HB\pm}^{h-1}\right]\,,$$

and we can conclude that p_3 is negative for all $h > 1$. Hence both Hopf bifurcations at $x_{HB\pm}$ are supercritical, and the dynamics consists of a stable equilibrium point outside the interval $g_{HB-} < g < g_{HB+}$ and a stable periodic oscillation for values of g within that interval. It is possible that additional periodic orbits are created within the interval $g_{HB-} < g < g_{HB+}$ through saddle-node bifurcations of periodic orbits, but this is not suggested in numerical experiments. Overall, the dynamics of the single-repressilator model (42) is that either the equilibrium (x_0, x_0, x_0) remains stable for all g, or that it undergoes two supercritical Hopf bifurcations, in which a stable periodic oscillation is created and then destroyed, as g increases.

5 Double-repressilator dynamics

As we noted in section 1, for the double-repressilator configuration there are two possibilities for the inhibitory interactions: either the two inhibitory influences can work independently of each other (so a high expression level of *either one or the other* TF suppresses expression), or a TF is suppressed only if *both* of the other TFs are strongly expressed. We refer to these two possibilities as the 'OR gate' and 'AND gate', respectively. The model (1) - (3) presented earlier describes the OR gate structure since the nonlinear interaction term, in, say, (1), is reduced below its typical value of around g if either x_2 or x_3 is large. In section 5.1 we discuss the dynamics of the OR gate case in detail, while in section 5.2 we present results for the alternative case, in which it is necessary for both of the other TFs to be highly expressed in order for the inhibitory mechanism to be switched on. The additional complexity of the double-repressilator model contrasts with the single-repressilator: here we find that the codimension-two point where the frequency of the Hopf bifurcation passes through zero provides the organising centre for the bifurcation structure.

5.1 Dynamics of the 'OR gate' model

In this section we compute explicitly the normal form coefficients p_j, q_j for the double-repressilator case studied in [16]. We specialise to the family of nonlinear terms proposed in (1) - (3) and use the normal form results to explain features of the bifurcation diagrams computed numerically in figures 2 and 3.

The observation that the results are essentially insensitive to the value of the coefficient b on the right-hand side of (1) - (3) since b is taken to be much smaller than the coefficients g and d. Hence we work here with the functional form

$$f(x_1, x_2, x_3) = \frac{g}{(1+\alpha x_2^h)(1+\beta x_3^h)} - dx_1\,, \tag{47}$$

where α, β, d, g and h are positive parameters. We observe that the partial derivatives of f are

$$f_1 = -d, \qquad f_2 = \frac{-\alpha g h x_2^{h-1}}{(1+\alpha x_2^h)^2(1+\beta x_3^h)}, \qquad f_3 = \frac{-\beta g h x_3^{h-1}}{(1+\alpha x_2^h)(1+\beta x_3^h)^2}\,.$$

Evaluating these at the symmetric equilibrium point (x_0, x_0, x_0) we see, as in the single-repressilator case, that there is no possibility of a steady-state bifurcation since $f_1 + f_2 + f_3$ is, again, always negative. The location of the fully-symmetric equilibrium (x_0, x_0, x_0) is defined by

$$(1+\alpha x_0^h)(1+\beta x_0^h)x_0 \;=\; \frac{g}{d}\,. \tag{48}$$

To locate the codimension-two point we set $\beta = \alpha$ so that f is symmetric in its second and third arguments and note that the Hopf bifurcation occurs when $f_1 = f_2 = f_3$, i.e. when

$$-d \;=\; -\frac{\alpha g h x_0^{h-1}}{(1+\alpha x_0^h)^3} = -\frac{\alpha d h x_0^h}{1+\alpha x_0^h}\,,$$

which implies that at the codimension-two point the equilibrium point takes the value

$$x_0 \;=\; \left(\frac{1}{\alpha(h-1)}\right)^{1/h} = \left(1-\frac{1}{h}\right)^2 \frac{g}{d}\,.$$

For the nonlinear terms we observe that, with the specific choice of functional form (47), several of the mixed derivatives vanish, for example $f_{11} = f_{12} = f_{13} = 0$. At the codimension-two point we see that the coefficients q_1, q_2 and q_3 all vanish due to the symmetry between the second and third arguments: subscripts equal to 2 or 3 are equivalent, in line with the discussion in section 2.2.

The Hopf bifurcation can be computed numerically by fixing values of α, β, d and h and solving simultaneously the two constraints (48) and $p_1 \equiv f_1 - f_2/2 - f_3/2 = 0$ to deduce values for g and x_0. The results for three values of h and a range of values of α, $10^{-4} \le \alpha \le 10^2$, are shown as

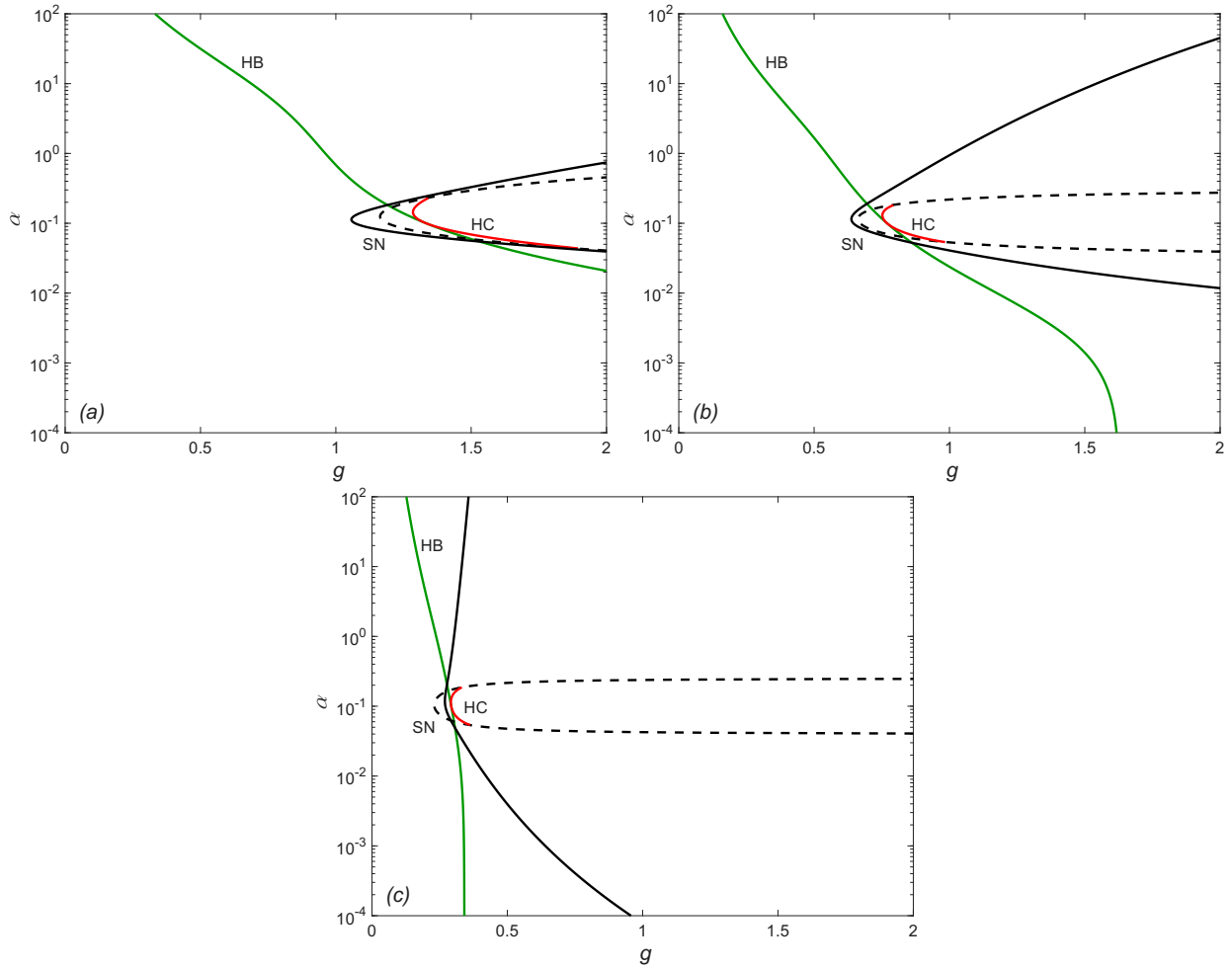

Figure 5: Bifurcation curves in the (g, α) plane for (a) $h = 2.4$; (b) $h = 3$; (c) $h = 7$. In each plot the Hopf bifurcation curve ('HB', solid green) and saddle-node bifurcation ('SN', solid black) are computed precisely. The heteroclinic bifurcation ('HC', solid red) and dashed black saddle-node curve use the approximations (18) and (22) which are accurate near the codimension-two point where the HB and HC curves meet. Other parameter values are: $\beta = 0.1$, $b = 0$, $d = 0.2$.

the green HB curves in figure 5. We see that at small h the Hopf bifurcation occurs at larger g when α is small, and at larger h the Hopf bifurcation moves to smaller g and its location becomes almost independent of α. Similarly, solving for the location of a non-symmetric equilibrium point undergoing a saddle-node bifurcation we obtain the solid black curves in figure 5 which indicate the location of the C-shaped saddle-node bifurcation curve, showing that it becomes less strongly curved as h increases.

For comparison, this figure also indicates the approximated form of the saddle-node (dashed black) and heteroclinic (red) bifurcation curves implied by the approximations (18) and (22) which are accurate only near the codimension-two point where the HB and HC curves meet. These approximations appear to be accurate in a larger region around the codimension-two point when h is small, and to be significantly inaccurate away from the codimension-two point when h is larger. In all cases, for values of g larger than those at the points where the HC and SN curves meet, the saddle-node bifurcations take place on the periodic orbit itself (i.e. a SNIC, or SNIPER, bifurcation) and the periodic orbit is destroyed. Figure 5(b) can be compared directly with the numerically-computed figure 3, validating the numerical results: the existence and organisation of the saddle-node, Hopf, and heteroclinic bifurcation curves is qualitatively exactly as predicted theoretically. Figure 5(b) illustrates that further from the codimension-two point, the bifurcation curves produced through the analysis near the codimension-two point tend to overestimate the size of the region in the (g, α) plane in which the periodic orbit exists (i.e. between the HB (green) and

SN (black) curves), and to underestimate the size of the region, inside the SN curve, that contains no periodic orbit and only the new equilibria that emerge in the saddle-node bifurcation.

Turning to the nonlinear description of these bifurcations, at the codimension-two point the expression for p_3 can be greatly simplified. First we note that, from the form of f proposed in (47) the expression for p_3 becomes

$$\begin{aligned} p_3 &= \frac{1}{4}\left(-f_{222} - f_{333} + \frac{(4f_{23} + 2f_{22} + 2f_{33})(f_{22} + f_{33} - f_{23})}{f_1 + f_2 + f_3}\right) \\ &= -\frac{1}{2}f_{222} - \frac{1}{3d}\left(f_{23} + f_{22}\right)\left(2f_{22} - f_{23}\right), \end{aligned} \tag{49}$$

using the fact that partial derivatives f_{22} and f_{33} are equal at the codimension-two point. After further algebraic manipulations we find that the expressions for f_{22}, f_{23} and f_{222} simplify dramatically at the codimension-two point and we obtain

$$f_{22} = \frac{d}{x_0}(3-h), \qquad f_{23} = \frac{d}{x_0} \qquad \text{and} \quad f_{222} = -\frac{d}{x_0^2}(h-2)(h-7), \tag{50}$$

and hence at the codimension-two point $\alpha = \beta$

$$p_3 = -\frac{d}{6x_0^2}(h-1)(h+2) = -\frac{d}{6}\alpha^{2/h}(h-1)^{1+2/h}(h+2) < 0, \tag{51}$$

and so the Hopf bifurcation near the codimension-two point is proved to be supercritical for all choices of the Hill function exponent h greater than unity. In fact, since the equilibrium point (x_0, x_0, x_0) exists only when $h > 1$, this result covers the whole range of possible choices of h and indicates that this part of the structure of the bifurcation diagram is independent of the choice of h.

The analytical result (51) is confirmed in figure 6(b) which plots the value of $-p_3 > 0$ along the Hopf bifurcation curves as shown in figure 5: we observe that p_3 is negative near $\alpha = 0.1 = \beta$ and indeed p_3 remains negative along the whole of the HB curve, showing that the Hopf bifurcation is always supercritical for these values of h. Further investigation (not shown here) suggests that the Hopf bifurcation may become mildly subcritical at values of α much smaller or larger than β when h is closer to unity. Figures 6(a) and (c) plot the normal form coefficients q_1 and q_3 respectively. q_1 is the frequency of small-amplitude periodic orbits near the Hopf bifurcation curve, while q_3 is the imaginary part of the coefficient of the cubic term in the normal form (12). It is interesting to observe that q_1 appears to depend only on the ratio α/β and appears to be an odd function of that ratio, while q_3 is clearly not. However, both q_1 and q_3 pass through zero at the codimension-two point $\alpha = \beta$, confirming what we anticipated from the theory set out in section 2.2, as discussed at the end of that subsection.

5.2 Dynamics of the 'AND gate' model

In the case in which high expression levels of two TFs are required in order to inhibit the expression of the third one, as discussed in [16] and that paper's supplementary material, an appropriate model is

$$\dot{x}_1 = b + \frac{g + g_2 x_2^h + g_3 x_3^h}{(1+\alpha x_2^h)(1+\beta x_3^h)} - d x_1 = f(x_1, x_3, x_3), \tag{52}$$

$$\dot{x}_2 = b + \frac{g + g_2 x_3^h + g_3 x_1^h}{(1+\alpha x_3^h)(1+\beta x_1^h)} - d x_2, \tag{53}$$

$$\dot{x}_3 = b + \frac{g + g_2 x_1^h + g_3 x_2^h}{(1+\alpha x_1^h)(1+\beta x_2^h)} - d x_3, \tag{54}$$

where, as previously, the parameters α, β, b, d, h, g, g_2 and g_3 are all taken to be positive. We consider g as our principal bifurcation parameter and note that the 'OR gate' form of the model

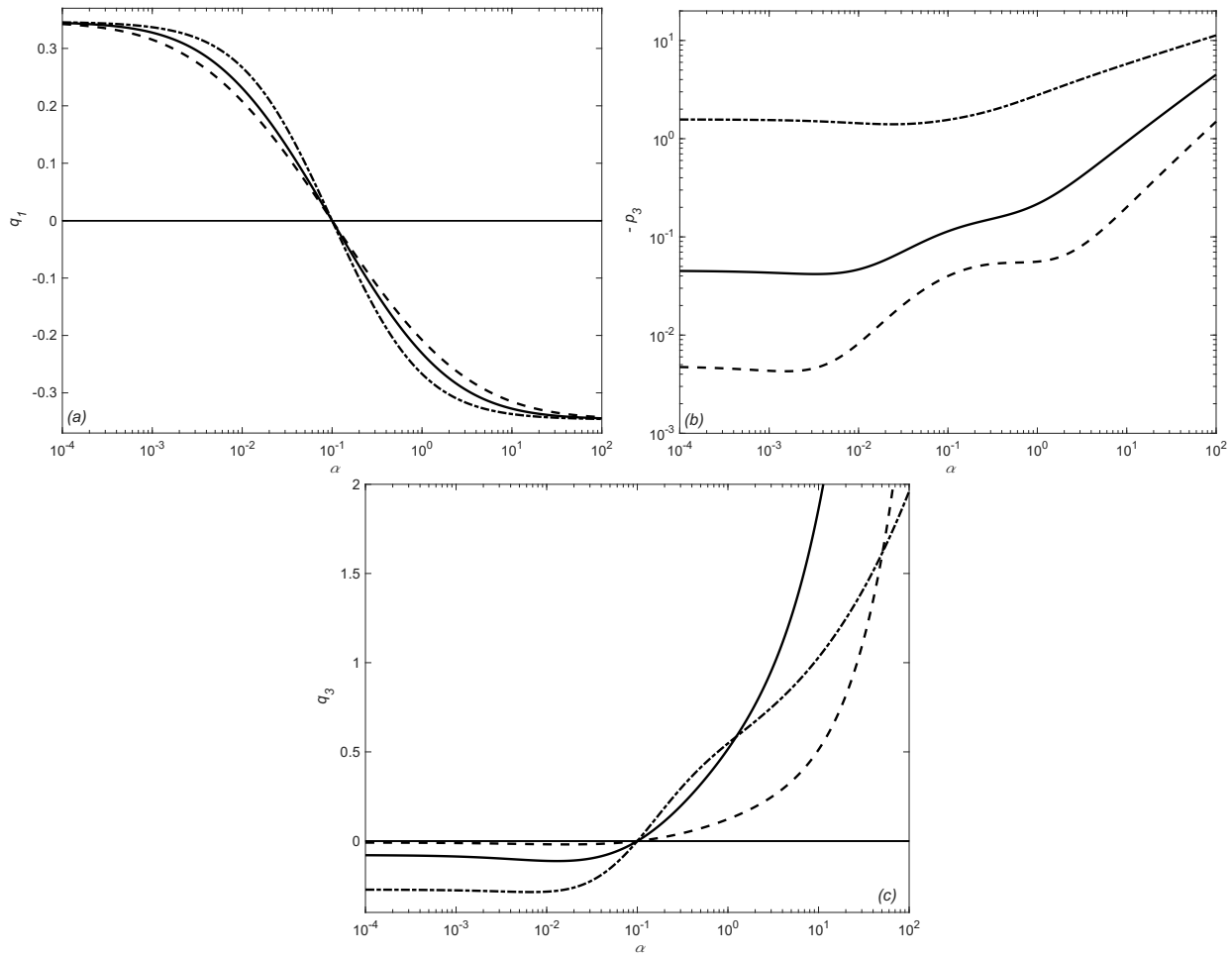

Figure 6: (a) Plot of the linear frequency of oscillations along the Hopf bifurcation curve shown in figure 5 in green, labelled 'HB', showing that the oscillation frequency passes through zero at $\alpha = \beta$. (b) Plot of the negative of the real part p_3 of the coefficient of the cubic term in the normal form (12), showing that $-p_3$ is positive (i.e. p_3 is negative) over the whole range of α shown here. (c) Plot of the imaginary part q_3 of the coefficient of the cubic term in the normal form (12) showing that this also vanishes at $\alpha = \beta$ as expected by symmetry. In each plot the dashed, solid and dash-dotted lines correspond to $h = 2.4$, $h = 3$ and $h = 7$, respectively. Other parameter values: $\beta = 0.1$, $b = 0$, $d = 0.2$.

corresponds to the case $g_2 = g_3 = 0$ and so in this sense the 'AND gate' can be considered a generalisation. In the analysis that follows we set $b = 0$ for convenience and because this constant background level of TF expression is likely to be small. Evaluating the partial derivatives of the right-hand side of (52), denoting this by $f(x_1, x_2, x_3)$, we obtain

$$\begin{aligned} f_1 &= -d\,, \\ f_2 &= \frac{g_2 h x_2^{(h-1)}}{(1+\alpha x_2^h)(1+\beta x_3^h)} - \frac{\alpha h x_2^{(h-1)}\left(g + g_2 x_2^h + g_3 x_3^h\right)}{(1+\alpha x_2^h)^2(1+\beta x_3^h)}\,, \qquad (55) \\ f_3 &= \frac{g_3 h x_3^{(h-1)}}{(1+\alpha x_2^h)(1+\beta x_3^h)} - \frac{\beta h x_3^{(h-1)}\left(g + g_2 x_2^h + g_3 x_3^h\right)}{(1+\alpha x_2^h)(1+\beta x_3^h)^2}\,, \qquad (56) \end{aligned}$$

Examining possibilities for symmetric equilibria (x_0, x_0, x_0) for (52) - (54) we see that there is always at least one equilibrium point when all parameters are positive. Unlike the 'OR gate' model, multiple equilibria are indeed possible (for example when $\alpha = \beta = d = 1.0$, $h = 3$, $g = 0.1$ and $g_2 = g_3 = 2.0$) and exist when $g_2 + g_3$ is sufficiently large. From this observation we expect that saddle-node bifurcations of symmetric equilibria occur for sufficiently large $g_2 + g_3$. Indeed,

evaluating (55) and (56) at a symmetric equilibrium we obtain

$$f_2 = \frac{(g_2 - \alpha g)hx_0^{(h-1)} - \alpha h g_3 x_0^{(2h-1)}}{(1+\alpha x_0^h)^2(1+\beta x_0^h)},$$
$$f_3 = \frac{(g_3 - \beta g)hx_0^{(h-1)} - \beta h g_2 x_0^{(2h-1)}}{(1+\alpha x_0^h)(1+\beta x_0^h)^2},$$

which shows that sufficient conditions to ensure $f_1 + f_2 + f_3 < 0$ (and so to rule out steady-state bifurcations) is that both $g_2 < \alpha g$ and $g_3 < \beta g$. When these inequalities are satisfied we are guaranteed a unique symmetric equilibrium point. We remark in passing that for (52) - (54) we do not require $g_2 = g_3$ for symmetric equilibria to exist since the location of symmetric equilibria depends only on the sum $g_2 + g_3$.

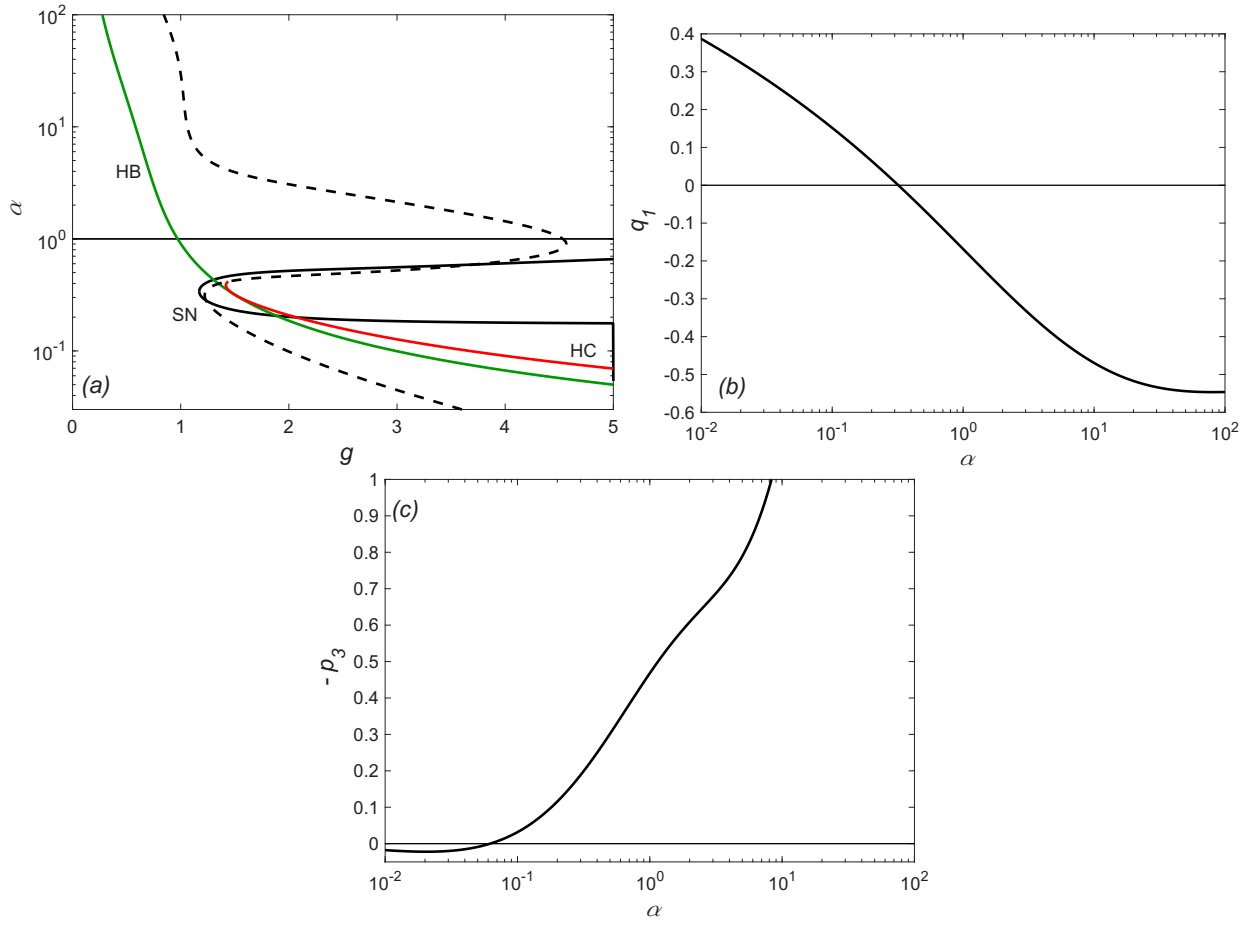

Figure 7: Analysis of the AND gate model (52) - (54) for $g_2 = 0.2$, $g_3 = 0.5$. (a) Bifurcation curves in the (g, α) plane, showing the Hopf bifurcation curve ('HB', solid green) and the saddle-node ('SN', solid black) computed numerically, together with the estimated locations of the saddle-node bifurcation (black dashed line) and heteroclinic bifurcation (red solid line) from the analysis near the codimension-two point. (b) Plot of the linear frequency q_1 against α along the Hopf bifurcation curve from (a), showing that q_1 passes through zero (defining the codimension-two point) at $\alpha \approx 0.3$. (c) Plot of the real part p_3 of the cubic term in (12) along the Hopf bifurcation curve from (a), showing that $p_3 < 0$ for $\alpha \gtrsim 0.06$ and hence the Hopf bifurcation is supercritical for this range of α. Other parameter values: $\beta = 1.0$, $b = 0$, $d = 0.3$.

Figures 7 - 9 illustrate the dynamics of the AND gate model for three typical combinations of the new parameters g_2 and g_3. In all cases we set the Hill exponent $h = 3.0$ to enable comparison with figure 5(b) and the solid curves in figure 6(a) and (b). Figure 7 shows the case $g_2 = 0.2$, $g_3 = 0.5$ which is qualitatively similar to the OR gate case (i.e. $g_2 = g_3 = 0$) discussed previously. The solid black curve is the numerically-computed saddle-node bifurcation which loops around the point on the Hopf bifurcation curve at which the linear frequency q_1 of the Hopf bifurcation passes

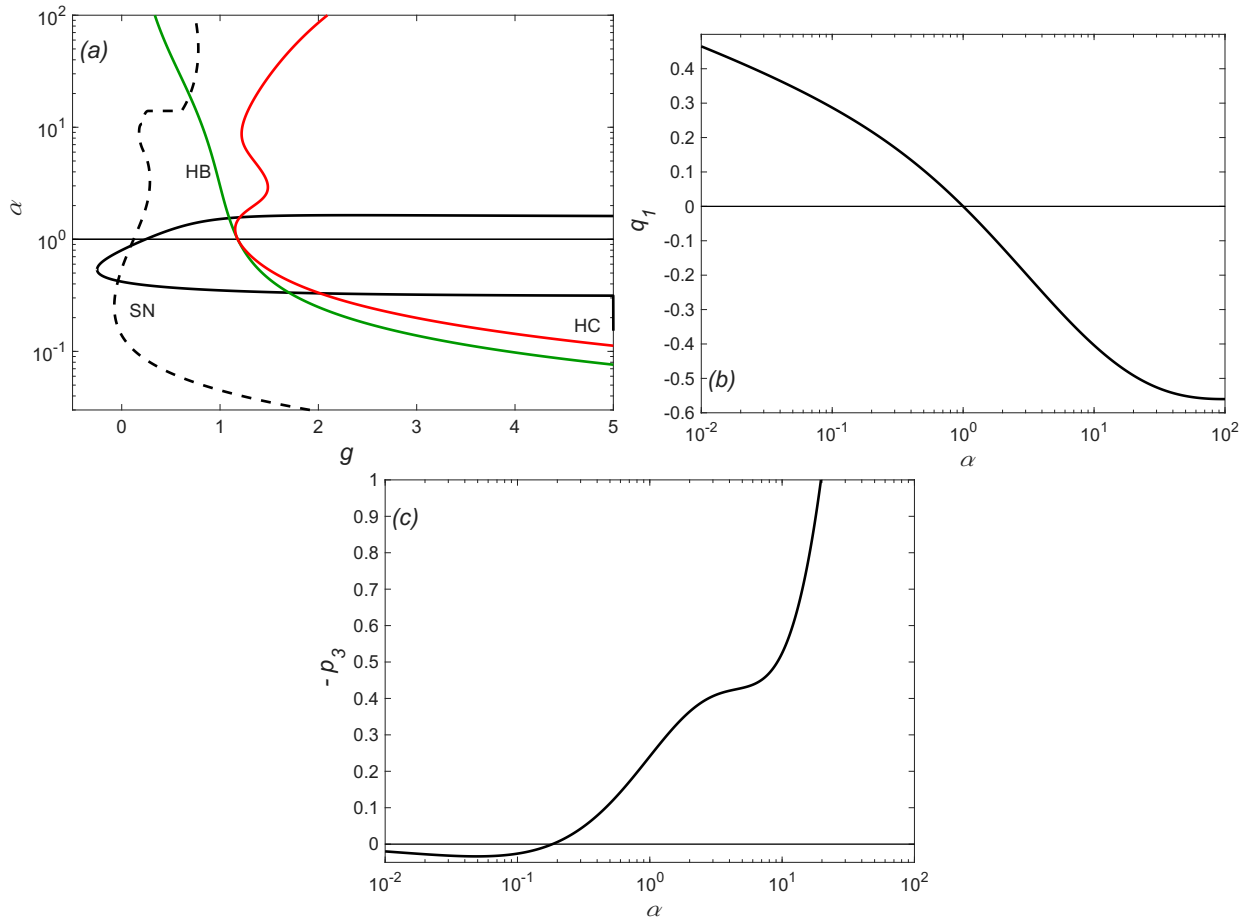

Figure 8: Analysis of the AND gate model (52) - (54) for $g_2 = g_3 = 0.7$. (a) Bifurcation curves in the (g, α) plane, showing the Hopf bifurcation curve ('HB', solid green) and the saddle-node ('SN', solid black) computed numerically, together with the estimated locations of the saddle-node bifurcation (black dashed line) and heteroclinic bifurcation (red solid line) from the analysis near the codimension-two point. (b) Plot of the linear frequency q_1 against α along the Hopf bifurcation curve from (a), showing that q_1 passes through zero (defining the codimension-two point) at $\alpha = 1$ (i.e. $\alpha = \beta$) as is expected for cases in which $g_2 = g_3$. (c) Plot of the real part p_3 of the cubic term in (12) along the Hopf bifurcation curve from (a), showing that $p_3 < 0$ for $\alpha \gtrsim 0.2$ and hence the Hopf bifurcation is supercritical for this range of α. Other parameter values: $\beta = 1.0$, $b = 0$, $d = 0.3$.

through zero. Since $g_2 \neq g_3$ the codimension-two point does not occur at $\alpha = \beta$ (corresponding to the horizontal solid line at $\alpha = 1$). But the analysis of the codimension-two point presented in section 2.3 does apply, near the point on the Hopf bifurcation curve where $\alpha \approx 0.3$ (figure 7b). The predictions for the saddle-node and heteroclinic bifurcations are shown as the dashed black and solid red curves, respectively. The dashed black curve is shown plotted for larger α, (i.e. for $\alpha > 1$) even though it is clearly unreliable so far from the codimension-two point. Figure 7(c) confirms that the Hopf bifurcation is supercritical near the codimension-two point and, indeed, for all values of α larger than approximately 0.06.

Turning to figure 8 for $g_2 = g_3 = 0.7$ we see that the shape of the Hopf bifurcation curve remains largely unchanged, but the saddle-node bifurcation shifts to smaller values of g. The turning point occurs when $g < 0$ where the model is unrealistic, but continuing the curves into $g < 0$ shows that the bifurcation structure remains qualitatively unchanged. Since in this case $g_2 = g_3$, and $\alpha = \beta$, we anticipate that the codimension-two point falls on the horizontal line that indicates $\alpha = \beta$ which is confirmed by the numerics. The dashed curve shows that the estimate provided by the analysis of section 2.3 is unreliable, as would be suggested by the separation between the accurate saddle-node curve (solid black curve) and the Hopf bifurcation curve itself. Figure 8(c) again confirms that the Hopf bifurcation remains supercritical for $\alpha \gtrsim 0.2$ and is only mildly subcritical for values of α

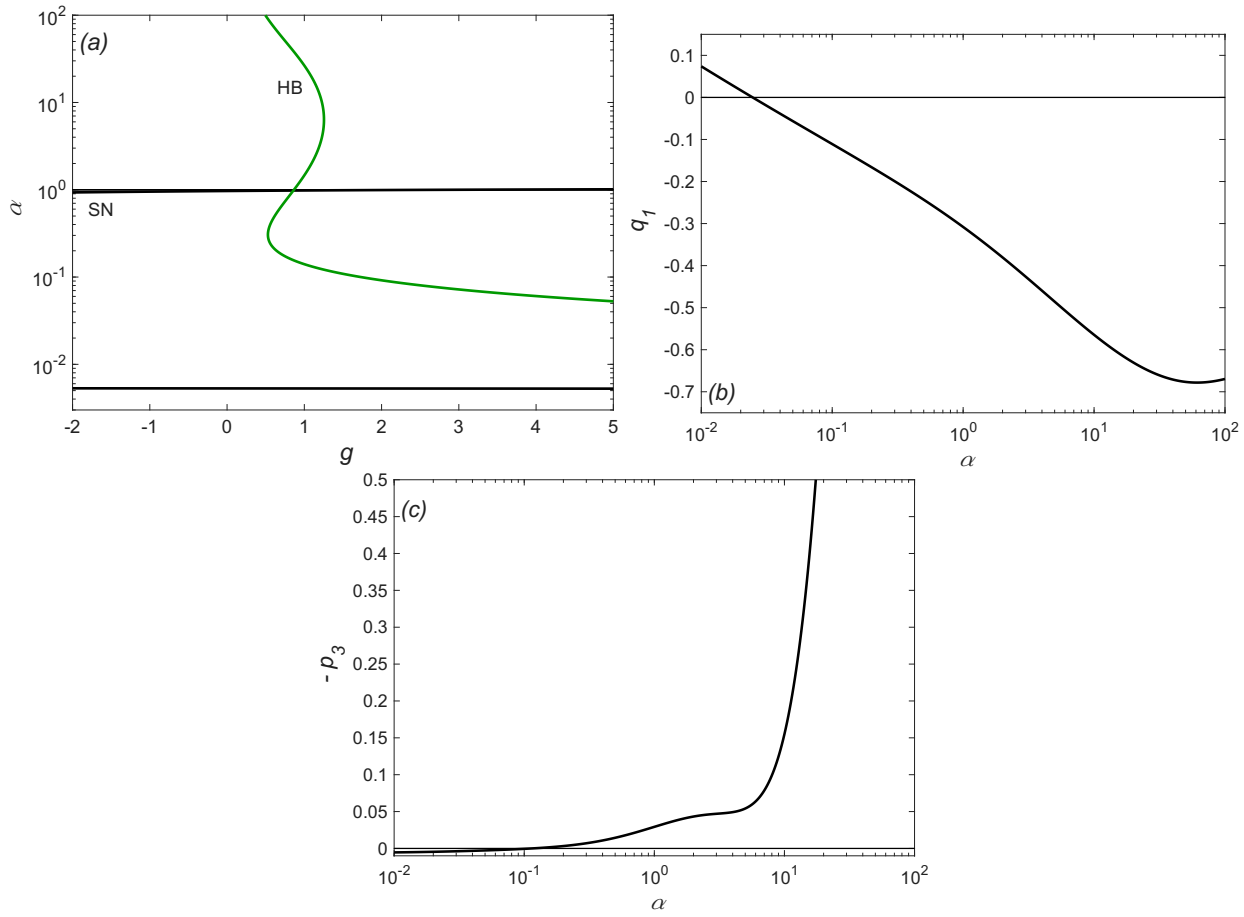

Figure 9: Analysis of the AND gate model (52) - (54) for $g_2 = 0.7$, $g_3 = 1.9$. (a) Bifurcation curves in the (g, α) plane, showing the Hopf bifurcation curve ('HB', solid green) and the saddle-node ('SN', solid black) computed numerically, and here taking the form of two almost-horizontal sections at $\alpha \approx 1.0$ and $\alpha \approx 0.005$. The estimates from the analysis near the codimension-two point are not shown due to their significant inaccuracy for these parameter values. (b) Plot of the linear frequency q_1 against α along the Hopf bifurcation curve from (a), showing that q_1 passes through zero (defining the codimension-two point) at $\alpha \approx 0.023$. (c) Plot of the real part p_3 of the cubic term in (12) along the Hopf bifurcation curve from (a), showing that $p_3 < 0$ for $\alpha \gtrsim 0.1$ and hence the Hopf bifurcation is supercritical for α larger than this, and subcritical for smaller α. Other parameter values: $\beta = 1.0$, $b = 0$, $d = 0.3$.

below that.

Lastly, figure 9 illustrates the case $g_2 = 0.76$, $g_3 = 1.9$; these parameter values are selected because they correspond to figure 10 in [16]. For such large values of g_2 and g_3 the saddle-node bifurcation curve has shifted much further towards more negative values of g, and appears here in two almost-horizontal pieces at $\alpha \approx 0.005$ and $\alpha \approx 1$. The Hopf bifurcation curve remains in the vicinity of $g = 1$ for $\alpha \gtrsim 0.1$ and then moves rapidly to much larger values of g. Due to the large separation between the turning point on the saddle-node curve and the codimension-two point on the Hopf bifurcation curve at which $q_1 = 0$ (at around $\alpha = 0.023$, corresponding to large positive g), we have not plotted here the approximations to the saddle-node and heteroclinic bifurcation curves since they will not be at all accurate in this case. Similar to the previous two figures, figure 9(c) indicates that the Hopf bifurcation is supercritical for small enough α, but in this case the Hopf bifurcation is subcritical for $\alpha \lesssim 0.1$, i.e. it is subcritical at the codimension-two point, and so the full bifurcation structure near the codimension-two point may well include additional bifurcations, for example a saddle-node bifurcation of periodic orbits.

In summary, at least for moderate values of g_2 and g_3, the dynamics of the AND gate model remains qualitatively similar to that of the OR gate model: at small g there is a stable symmetric equilibrium point which is destabilised through a supercritical Hopf bifurcation, before new non-

symmetric equilibria are created at a saddle-node bifurcation curve which is 'C-shaped' in the (g, α) plane. Outside the saddle-node curve we expect the oscillatory behaviour to remain stable.

6 Discussion and conclusions

We have carried out a thorough mathematical analysis of the model (1) - (3) that was proposed to describe the process through which gene interactions can drive cell differentiation - the Cyclical Fate Restriction (CFR) hypothesis, aiming the reconcile the evidence that is proposed to support the Direct Fate Restriction or Progressive Fate Restriction models. What is perhaps most important in general is our conclusion concerning the robustness of the dynamics of the CFR model. Almost regardless of the choices of the interaction parameters α and β, the (small) constant production and degradation rates b and d, and the Hill function exponent h, the behaviour of the model ODEs is to move between a stable symmetric equilibrium where all TFs are equally expressed, to a state where new equilibria in which the expression levels of the three TFs differ emerges at large g, with an intermediate regime that is integral to the dynamics where stable time-periodic oscillations exist. The time-periodic oscillations appear at a standard Hopf bifurcation but disappear at a global bifurcation involving the new asymmetric equilibria: this is a heteroclinic bifurcation close to the codimension-two point, or a saddle-node-on-a-periodic-orbit (SNIPER, also referred to as a saddle-node-invariant-circle, SNIC, bifurcation) further away. The characteristics of a SNIPER bifurcation, in which the period of the oscillations becomes longer while their amplitude remains constant, are sufficiently distinctive to be observable in experiments [25].

We have shown that this sequence of bifurcations holds for both the 'OR gate' version of the model (1) - (3), in which either of the other TFs can inhibit the production of the third TF, and for the 'AND gate' version (52) - (54) in which high expression levels of both TFs are required.

The symmetry of the system, in which the coordinates can be permuted cyclically, is motivated by an underlying assumption that there are a number of roughly equally-likely differentiation pathways available to the multipotent cell. Of course exact equality is very unlikely (and can be captured easily through variation of the problem parameters b, d, g or the interactions α and β between the three equations in the model (1) - (3)), but a mathematical model that starts from this premise is much easier to perturb away from the fully-symmetric form, than to formulate one in which, for example, two of the TFs dominate and a third is only weakly coupled. Having started with this permutation symmetry, in section 2.1 we showed that there were only two possible generic bifurcations that destabilise the fully-symmetric equilibrium point: either a local steady-state bifurcation (which could in general be a saddle-node, transcritical or pitchfork bifurcation) corresponding to perturbations that preserve the cyclical symmetry, or a Hopf bifurcation that involves different eigenvectors because it corresponds to a different irreducible representation of the $\mathbb{Z}_3$ symmetry group. This insight will also organise bifurcations for similar models with larger numbers of interacting TFs. The relevant symmetry group will depend on the number of TFs and the form of the interactions between them and opens up interesting directions for future work. The relevant representation theory is well-known and leads immediately to the expectations of similar results to those presented here, for example because all the irreducible representations of $\mathbb{Z}_n$ are either one-dimensional or two-dimensional and so the possibilities remain very similar to the $\mathbb{Z}_3$ case analysed here.

The systematic analysis of symmetry-breaking perturbations is a substantial topic that we leave for future work. We included a brief discussion of the typical effects in our previous paper [16]; see section 3.2 and figure 9 in that paper. From general dynamical systems theory we expect that the Hopf and saddle-node bifurcations will persist when the $\mathbb{Z}_3$ symmetry is weakly-broken. In the symmetric case the saddle-node bifurcation corresponds to three separate bifurcations and these will occur on distinct but nearby curves in parameter space in the weakly-asymmetric case. As shown numerically in [16] the heteroclinic bifurcation will then involve only a single saddle point, or nonhyperbolic saddle-node-type equilibrium, rather than colliding with all three at the same parameter value as in the symmetric case. Overall, the effect of the broken symmetry will still be that the periodic orbit disappears; potentially there will be a region in parameter space where

only one or two, and not all three, new asymmetric stable equilibria exist. In biological terms symmetry-breaking therefore suggests a mechanism for guaranteeing that one cell fate pathway is favoured over others.

Moving on to the dynamics of the problem, our analysis reveals that the new equilibria and the periodic orbit are closely linked, in the sense that they are both generated through bifurcations that form part of the generic behaviour of the model near the codimension-two point where the frequency of the periodic orbit produced in the Hopf bifurcation passes through zero.

For the OR gate model (1) - (3) we have shown here numerically that for reasonable choices of the problem parameters the Hopf bifurcation is always supercritical. Further, mathematical analysis proves that, for all values of $h > 1$ (where the model is well-posed) the Hopf bifurcation is supercritical near the codimension-two point at $\alpha = \beta$. Figure 6(b) suggests that p_3 becomes even more negative as h increases: large h corresponds to the formation of multimers of increasing size and is associated with the Hopf bifurcation becoming more strongly supercritical. The same appears to be true for the AND gate model (52) - (54) in a large region around the codimension-two point where the frequency of the Hopf bifurcation passes through zero.

Looking even more widely, the effects of symmetry remain the same regardless of the precise modelling paradigm, and there is plenty of scope for the results presented here, for example the centre manifold reduction results captured by (36) - (41) to be applicable to systems with the same symmetry properties but quite different biological or physical motivation. This centre manifold reduction does not appear to be easily at hand in the literature and is one reason that we present it is substantial detail, albeit deferring much of that to the Appendix.

The analysis of the normal form (12) is a further case in point. Although it would be extremely surprising if the results of section 2.3 were new (indeed at least some aspects of the analysis go back over forty years to [1]), we have been unable to find a sufficiently detailed and complete account to refer the reader to which is why we have presented details of the derivation of these results here, and not just the results themselves, in the expectation that they will be of use elsewhere.

Turning back to the original biological setting, we note that it should now be straightforward to apply these results to a number of variations of the model, including breaking of the exact symmetry between the TFs, including a larger number of TFs, introducing alternative coupling topologies between the TFs, introducing additional variables, and changing the form of the (inhibitory) interaction term. On this last point we note that we have not carried out a complete bifurcation analysis of the AND gate model (52) - (54) since it contains a larger number of parameters and additional kinds of behaviour occur, for example the occurrence of multiple symmetrical equilibria for which $x_1 = x_2 = x_3$. A more detailed discussion of the AND gate model is left for future work.

Conceptually, our work represents a departure from the Waddington paradigm in one important respect: we place emphasis on the ability of the cyclical nature of the inhibitory interactions in our model to generate temporal oscillations. Formally this prevents the construction of an 'energy landscape' on which the dynamics can be that of a ball rolling strictly downhill - in more physical terms, there is no energy potential that the system is seeking, through its dynamics, to minimise (i.e. a gradient flow). The construction, and consequences, of a gradient-flow formalism and the related generic bifurcation theory has been explored in considerable detail [8, 28, 29, 30]. There are strong similarities in philosophy between our work and these papers, not least that *a priori* classification of the possible dynamical scenarios and and understanding of the generic qualitative changes between them is a useful approach to building insight into the biology. The differences are, first, that given our starting point – the role of symmetry, and exploring the consequences of mutual inhibition – our aim has been to understand the bifurcation behaviour of this class of models specifically. This has led, second, to the need to understand and include the intermediate states between initial and final equilibria (i.e. the multipotent and fate-differentiated final states, respectively) and explore their possible role in resolving the argument between the Progressive Fate Restriction (PFR) and Direct Fate Restriction (DFR) models as outlined in the introduction and described in much more detail in [23]. The analyses share the feature of being concerned with structurally stable (Morse–Smale) systems and the bifurcation analysis presented here expands and builds on what would be obtained by working just with the directed acyclic graph built from initial and final equilibria [28] in order

to understand the consequences at intermediate times for gene expression levels, not assuming that these rise or fall monotonically along cell fate choice pathways. Indeed, [28] discusses a three-state model with mutual inhibition in section 3A and in its supplementary material, in section II.1, in a form qualitatively identical to (1) - (3) but parameterised differently, since the focus in that paper is on exploring all possible forms of symmetry-breaking away from the fully-symmetric configuration. These symmetry-breaking pathways would correspond to Progressive Fate-Restriction (PFR) events in which TF expression levels evolved monotonically to indicate transitions between stable or at least metastable states, whereas the appearance of the intermediate oscillatory regime would allow a scenario to be observed that looked more similar to Direct Fate Restriction, with a number of new cell types emerging after a complicated intermediate, and inherently dynamical, regime. These approaches therefore appear to be complementary.

Finally, we remark that the well-established occurrence of time-periodic oscillations in gene regulatory dynamics, in a number of distinct settings, [26, 27, 9, 5] suggests that they may, at least in certain situations, contribute in ways not yet fully appreciated to the timing or selection of cell fates, while continuing to provide significant challenges to experimental methodology.

Acknowledgements

This work was supported by the Biotechnology and Biological Sciences Research Council, part of UKRI [grant numbers BB/S01604X/1 and BB/S015906/1].

References

[1] Arnold VI. 1980 *Chapitres supplémentaires de la théorie des équations differentielles ordinaires.* Editions Mir, Moscow.

[2] Briscoe J, Small S. 2015 Morphogen rules: design principles of gradient-mediated embryo patterning. *Development* **142**, 3996–4009.

[3] Broer HW, van Dijk R, Vitolo R. 2008 Survey of strong normal-internal $k : \ell$ resonances in quasi-periodically driven oscillators for $\ell = 1, 2, 3$. In *SPT 2007 – Symmetry and perturbation theory*, pages 45-55. World Sci. Publ., Hackensack, NJ.

[4] Brombin A, Patton EE. 2024 Melanocyte lineage dynamics in development, growth and disease *Development* **151**, dev201266.

[5] Burton J, Manning CS, Rattray M, Papalopulu N, Kursawe J. 2021 Inferring kinetic parameters of oscillatory gene regulation from single cell time-series data. *J. R. Soc. Interface* **18**:20210393.

[6] Chossat P, Lauterbach R. 2000 *Methods in Equivariant Bifurcations and Dynamical Systems.* Advanced Series in Nonlinear Dynamics, volume 15. World Scientific.

[7] Cohen M, Page KM, Perez–Carrasco R, Barnes CP, Briscoe J. 2014 A theoretical framework for the regulation of Shh morphogen-controlled gene expression. *Development* **141**, 3868–3878.

[8] Corson F, Siggia ED. 2017 Gene-free methodology for cell fate dynamics during development. *eLife* **6**, e30743.

[9] Cutillo L, Boukouvalas A, Marinopoulou E, Papalopulu N, Rattray M. 2020 OscoNet: inferring oscillatory gene networks. *BMC Bioinformatics* **21**(Suppl 10):351.

[10] Dawes JHP, Kelsh RN. 2021 Cell fate decisions in the neural crest, from pigment cell to neural development. *Int. J. of Mol. Sci.* **22**(24).

[11] Dey A, Barik D. 2021 Potential landscapes, bifurcations, and robustness of tristable networks. *ACS Synth. Biol.* **10**, 391-401.

[12] van Dijk R. 2007 Master's thesis. Universiteit Groningen.

[13] Elowitz MB, Leibler S. 2000 A synthetic oscillatory network of transcriptional regulators. *Nature* **403**, 335–338.

[14] Erickson AG, Kameneva P, Adameyko I. 2023 The transcriptional portraits of the neural crest at the individual cell level. *Seminars in Cell and Developmental Biology* **138**, 68-–80.

[15] Fagan MB. 2016 Stem cells and systems models: clashing views of explanation. *Synthese* **193**, 873–907.

[16] Farjami S, Camargo Sosa K, Dawes JHP, Kelsh RN, Rocco A. 2021 Novel generic models for differentiating stem cells reveal oscillatory mechanisms. *J. Roy. Soc. Interface*, **18**(183):20210442

[17] Gambaudo JM. 1985 Perturbation of a Hopf bifurcation by an external time-periodic forcing. *J. Diff Eqns.* **57**, 172–199.

[18] Golubitsky M, Stewart I. 2002 *The Symmetry Perspective: From Equilibrium to Chaos in Phase Space and Physical Space.* Progress in Mathematics, Volume **200**. Springer, Basel.

[19] Golubitsky M, Stewart IN, Schaeffer DG. 1988 *Singularities and Groups in Bifurcation Theory vol II.* Applied Mathematical Sciences Series Volume **69**. Springer, Berlin.

[20] Hoyle R. 2006 *Pattern Formation: An Introduction to Methods.* Cambridge University Press, Cambridge.

[21] Kaneko K. 2011 Characterisation of stem cells and cancer cells on the basis of gene expression profile stability, plasticity, and robustness. *Bioessays* **33**, 403-–413.

[22] Kaity B, Sarkar R, Chakrabarti B, and Mitr MK. 2018 Reprogramming, oscillations and transdifferentiation in epigenetic landscapes. *Scientific Reports* **8**:7358.

[23] Kelsh RN, Camargo Sosa K, Farjami S, Makeev V, Dawes JHP, Rocco A. 2021 Cyclical fate restriction: a new view of neural crest cell fate specification. *Development*, **148**(22).

[24] Kharchenko PV. 2021 The triumphs and limitations of computational methods for scRNA-seq. *Nature Methods* **18**, 723–732.

[25] Meeuse MWM, Hauser YP, Morales Moya LJ, Hendriks G-J, Eglinger J, Bogaarts G, Tsiairis C, Großhans H. 2020 Developmental function and state transitions of a gene expression oscillator in *Caenorhabditis elegans*. *Mol. Syst. Biol.* **16**:e9498.

[26] Niwa Y, Shimojo H, Isomura A, González A, Miyachi H, Kageyama R. 2011 Different types of oscillations in Notch and Fgf signaling regulate the spatiotemporal periodicity of somitogenesis. *Genes & Development* **25**, 1115-–1120.

[27] Page KM. 2019 Oscillations in well-mixed, deterministic feedback systems: Beyond ring oscillators. *J. Theor. Biol.* **481**, 44–53 (2019)

[28] Rand DA, Rajub A, Sáez M, Corson F, Siggia ED. 2021 Geometry of gene regulatory dynamics. *PNAS* **118**(38) e2109729118.

[29] Sáez M, Briscoe J, Rand DA. 2022 Dynamical landscapes of cell fate decisions. *Interface Focus* **12**:20220002.

[30] Sáez M, Blassberg R, Camacho-Aguilar E, Siggia ED, Rand DA, Briscoe J. 2022 Statistically derived geometrical landscapes capture principles of decision-making dynamics during cell fate transitions. *Cell Systems* **12**, 12–28.

[31] Subkhankulova T, Camargo Sosa K, Uroshlev LA, Nikaido M, Shriever N, Kasianov AS, Yang X, Rodrigues FSLM, Carney TJ, Bavister G, Schwetlick H, Dawes JHP, Rocco A, Makeev VJ, Kelsh RN. 2023 Zebrafish pigment cells develop directly from persistent highly multipotent progenitors. *Nature Communications* **14**:1258.

[32] Vo HK, Dawes JHP, Kelsh RN. 2024 Oscillatory differentiation dynamics fundamentally restricts the resolution of pseudotime reconstruction algorithms. *J. Roy. Soc. Interface* **21**:20230537.

[33] Waddington CH. 1940 *Organisers and Genes*. Cambridge University Press.

[34] Zhou JX, Huang S. 2011 Understanding gene circuits at cell-fate branch points for rational cell reprogramming. *Trends in Genetics* **27**(2), 55–62.